ELECTRON CONTENT OF BARIUM PLASMAS IN THE HIGH ATMOSPHERE

Raymond E. Prenatt, et al

Ballistic Research Laboratories
Aberdeen Proving Ground, Maryland

December 1969

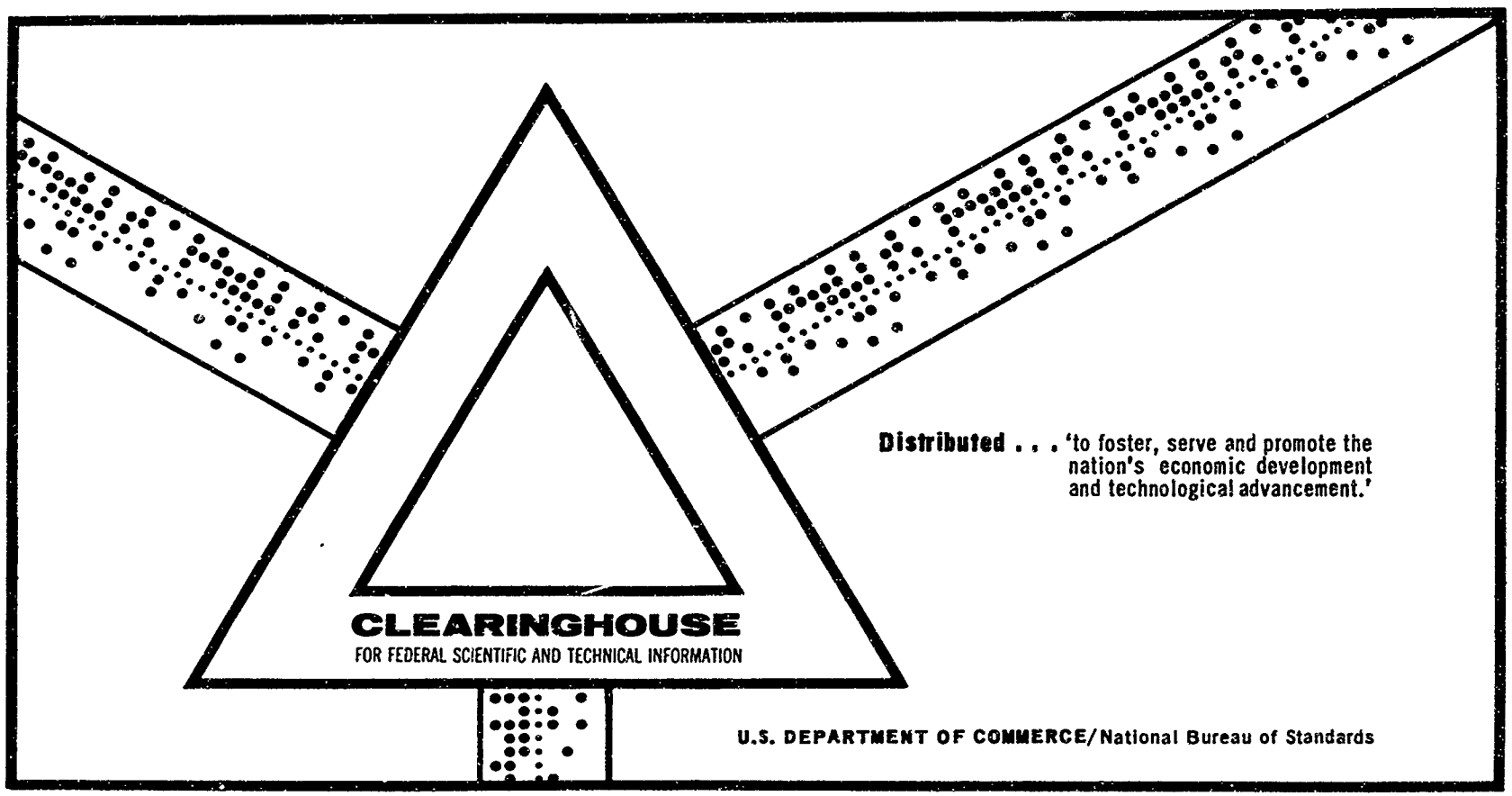

BRL R 1459

BRL

REPORT NO. 1459

ELECTRON CONTENT OF BARIUM PLASMAS IN THE HIGH ATMOSPHERE

by

Raymond E. Prenatt
William A. Dean
Warren W. Berning

December 1969

U.S. ARMY ABERDEEN RESEARCH AND DEVELOPMENT CENTER
BALLISTIC RESEARCH LABORATORIES
ABERDEEN PROVING GROUND, MARYLAND

Destroy this report when it is no longer needed.
Do not return it to the originator.

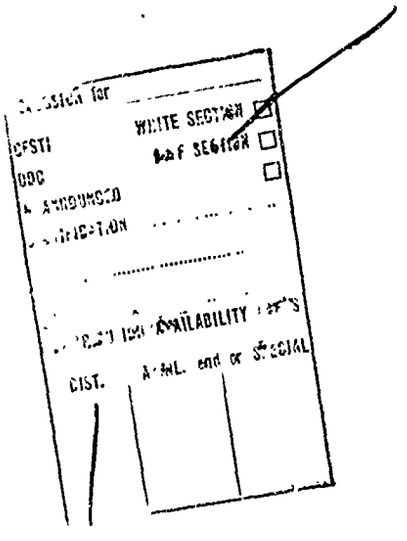

The findings in this report are not to be construed as an official Department of the Army position, unless so designated by other authorized documents.

B A L L I S T I C R E S E A R C H L A B O R A T O R I E S

REPORT NO. 1459

DECEMBER 1969

ELECTRON CONTENT OF BARIUM PLASMAS IN THE HIGH ATMOSPHERE

Raymond E. Prenatt
William A. Dean

Signature and Propagation Laboratory

Warren W. Berning

Defense Atomic Support Agency

RDT&E Project No. 5910.21.61083

A B E R D E E N P R O V I N G G R O U N D, M A R Y L A N D

B A L L I S T I C R E S E A R C H L A B O R A T O R I E S

REPORT NO. 1459

REPrenatt/WADean/WWBerning/n11
Aberdeen Proving Ground, Md.
December 1969

ELECTRON CONTENT OF BARIUM PLASMAS IN THE HIGH ATMOSPHERE

ABSTRACT

At evening twilight on 4 October 1967 a rocket carrier released three barium clouds off Wallops Island, Virginia. The vehicle also carried a multifrequency VHF beacon for the observation of radio frequency dispersive phase and amplitude variations in signals propagated through the release clouds, and as a derived quantity, total electron content along the propagation paths. The first cloud, at 103 kilometers, introduced no measurable dispersive phase variations and only a brief decrease in signal strength. The other clouds at 187 and 226 kilometers produced large and unusual effects on both dispersive phase and signal strength data.

Analysis of the dispersive phase data obtained during rocket descent, when the rocket had emerged from behind the release clouds, yielded a normal electron density profile. A preliminary attempt at interpreting the data relevant to the second release employed ray tracing through spherically symmetric, diffusing cloud models with a gaussian electron density distribution. By varying the parameters defining the cloud, a model was devised that closely duplicated both the dispersive phase and signal strength data.

TABLE OF CONTENTS

LIST OF TABLES

LIST OF ILLUSTRATIONS

I. INTRODUCTION

The general subject of and specific experiments relating to chemical releases at very high altitudes have been well reviewed in the literature (Bates, 1950; Rosenberg and Golomb, 1963; Rosenberg, 1966; Lloyd and Sheppard, 1966; Foppl, et al, 1967; Haerendel and Lust, 1968a; Haerendel and Lust, 1968b). The element, barium, as a release constituent has proven of particular interest because it ionizes readily in sunlight and the ion possesses strong resonant scattering lines in the visible and near-visible part of the spectrum. The formation of easily observable barium plasmas at high altitudes has proven very useful in the determination of vector electric fields present, and in the generation of magnetic field-aligned ion density inhomogeneities (tentatively attributed to the development of large-scale plasma instabilities).

For experiments in which a marked disturbance of the high altitude natural environment is desired, there is interest in release particle densities of perhaps $10^8 cm^{-3}$ in a volume of 500 km^3. If the particle desired is the barium ion and an efficiency of 10% is assumed in converting vaporizable barium to the barium ion via solar ionization, chemical releases containing approximately 1000 moles (137 kg) of vaporizable barium are required. A chemical release of this magnitude is no trivial problem. For diagnostic purposes it becomes important to know the release densities achieved and the density distribution in the release volume. Appropriate measurements of these parameters may derive from observations of spectral line (or band) emission and, for plasmas, from observations of radio wave signals propagated through or scattered from the plasma cloud or from direct probe measurements in the plasma. Unfortunately, a barium ion plasma of the density and extent here indicated is optically thick for a substantial period of time in the prominent barium ion transitions driven by solar excitation. For even the hyperfine emission arising from the presence of barium isotopes, the cloud is optically thick at early times. Thus, radio wave or direct probe measurements are important in determining the early time properties and formation of plasmas resulting from chemical releases.

In late 1966, the Ballistic Research Laboratories (BRL) were invited to participate in the chemical release experiment to be conducted by the Air Force Cambridge Research Laboratories (AFCRL). The experiment encompassed the launching of two sounding rockets and payloads, each containing three barium release canisters for deployment at different altitudes. The BRL participation consisted of instrumenting the nose section of each vehicle with a multifrequency VHF beacon for transmission downward through the release plasma, and for operating and servicing the rocket and ground equipments in the field. The experiments were conducted at evening twilight on 3 and 4 October 1967, with vehicle launchings from Wallops Island, Virginia. The flights were given the code names URSULA and VERA, respectively. The chemical releases, six in number occurred at or near the programmed altitudes. The BRL radiowave experiment failed early in flight on 3 October (attributed to a payload shroud failure) but operated successfully during the flight on 4 October. The following sections discuss the nature of the BRL experiment and the results obtained from the 4 October flight (VERA).

II. THE VHF EXPERIMENT

The propagation experiment employed a three-frequency beacon carried in the nose cone of the chemical release rocket. Significant characteristics of the transmitting and receiving system are given in Table I. Figures 1 and 2 show the rocket payload components and configuration similar to those employed in the experiment here described. A discussion of very similar instrumentation and its use in studies of the ionosphere may be found in publications of the BRL (Dean, et al, 1968). The signals received on the ground are electronically processed as shown in Figure 3, and the processed information stored on paper chart and magnetic tape for subsequent analysis and computer processing. For VERA the 583 MHz transmission was not employed.

In operation, the beacon transmits continuously as the rocket rises. Upon release of the chemical, the transmitter is first enveloped by the chemical then rises above the release cloud and transmits through the

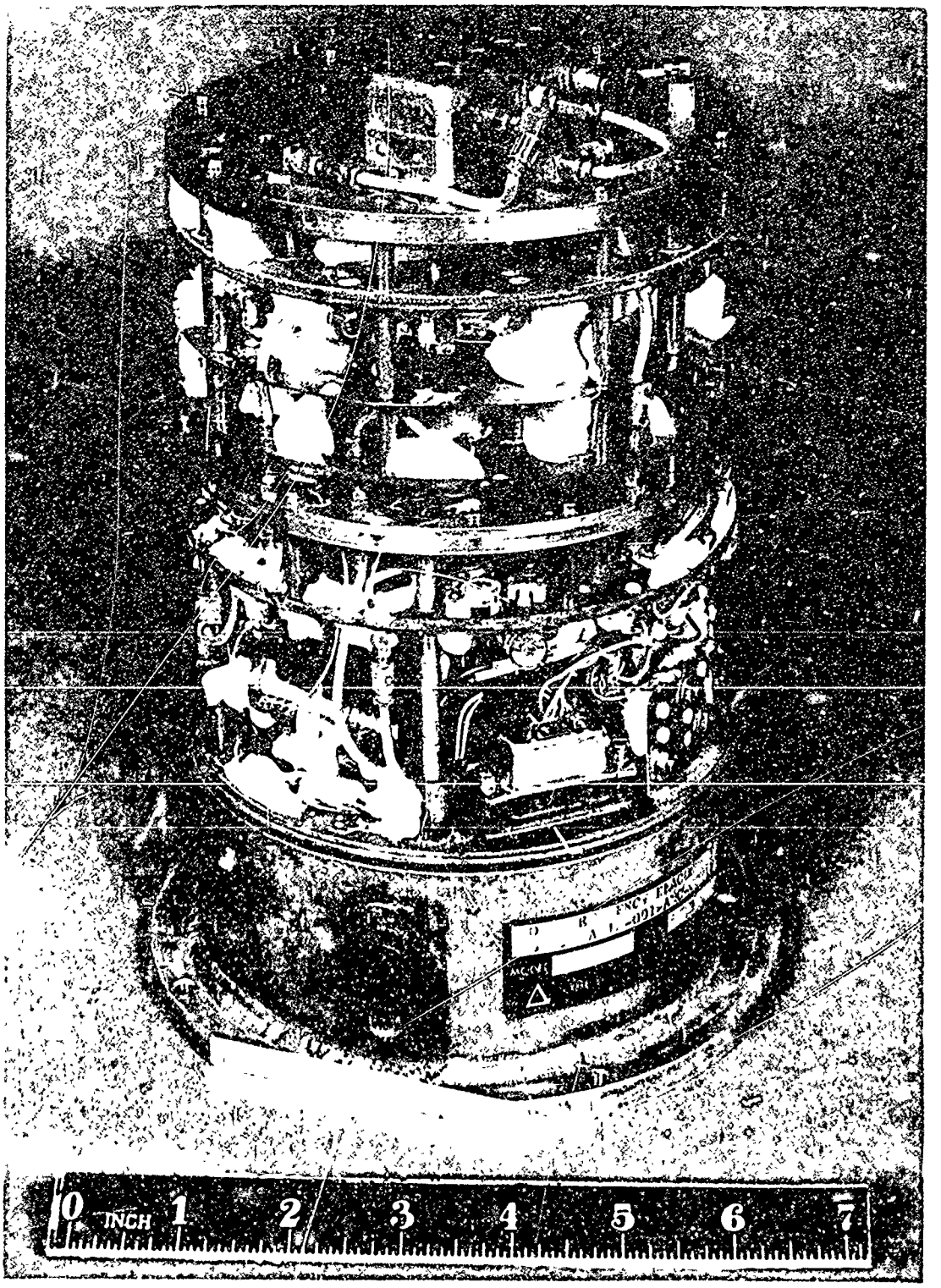

Figure 1. Four – Frequency Propagation Beacon With Case Removed.

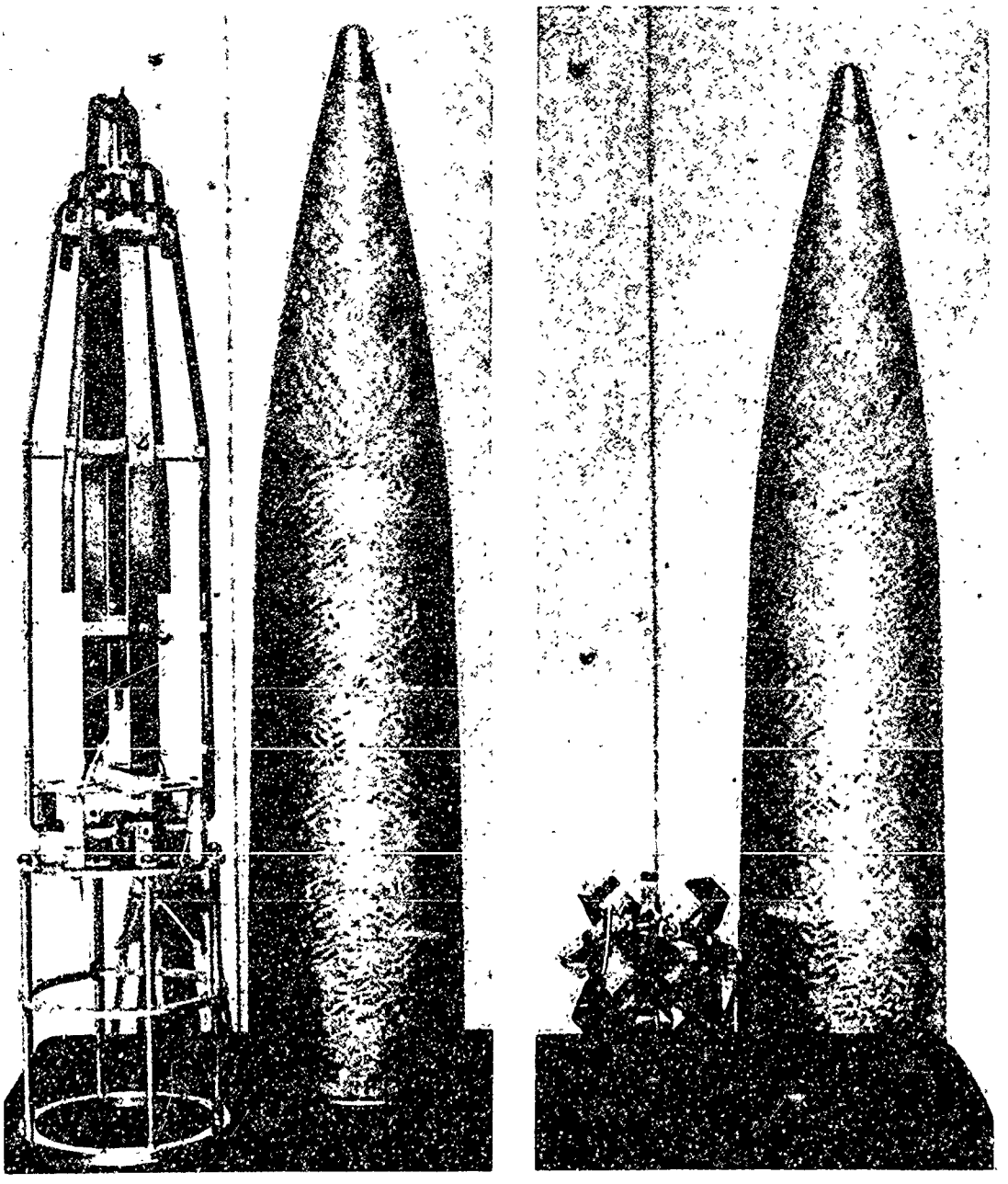

Figure 2. Rocketborne Antennas for Four-Frequency Beacon.

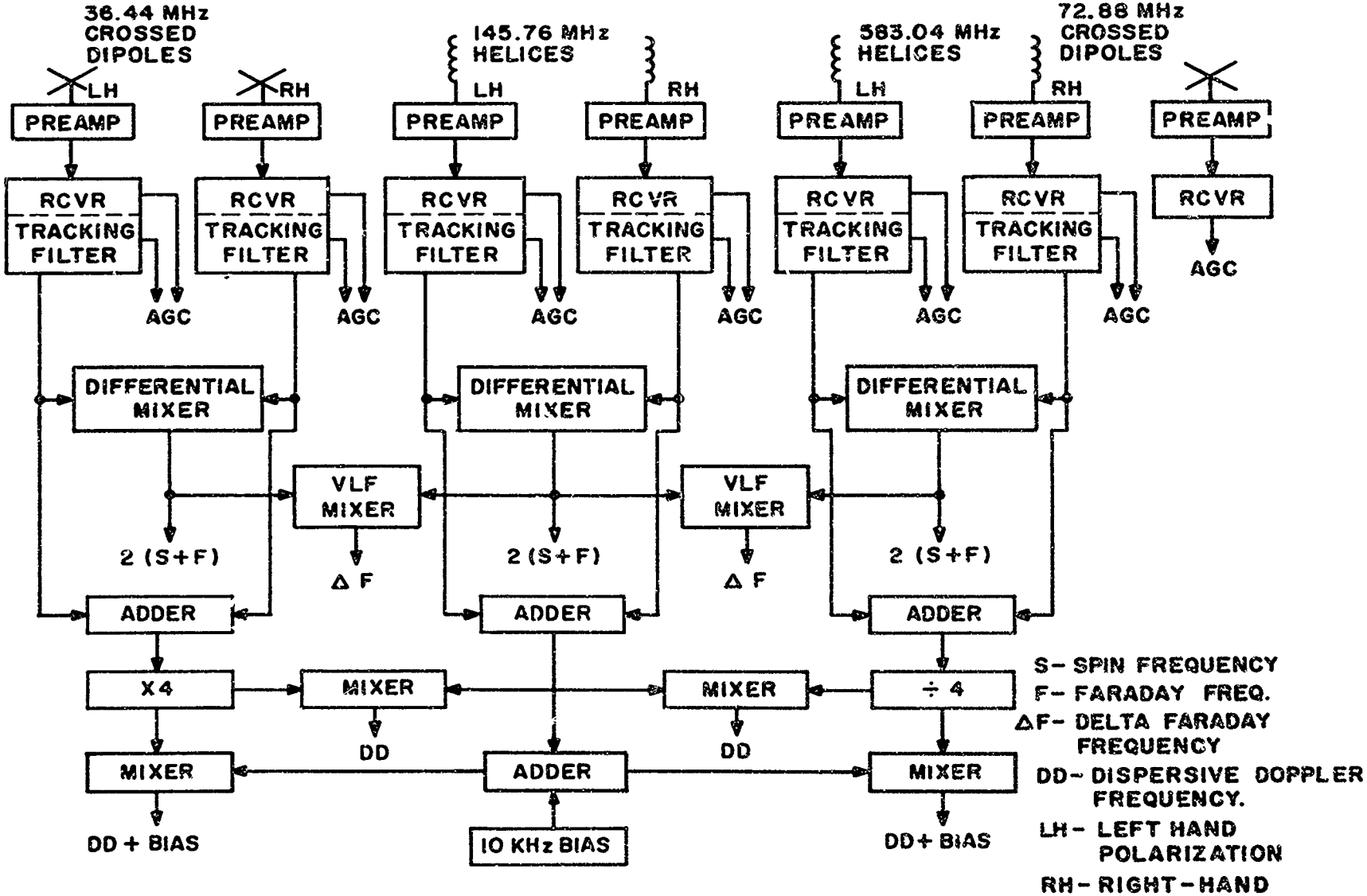

Figure 3. Block Diagram of Four Frequency Ground Station.

Table I. Characteristics of Propagation Experiment Equipments

Transmitter

Frequency: 36.44 MHz, 72.88 MHz and 145.76 MHz

Operating Mode: CW

Power Output: 130 mw at 36.44 MHz
260 mw at 72.88 MHz
105 mw at 145.76 MHz

Rocketborne Antennas

Type: Loops at 36.44 MHz and 72.88 MHz
Folded dipole at 145.76 MHz

Beam Width: A minimum of 90 degrees at all frequencies, (plus and minus 45 degrees), with a major pattern lobe directed to the rear along the longitudinal axis of the rocket with a maximum variation of less than ±1.5 db within the beam width cone.

Polarization: Linear with antenna axis prependicular to rocket longitudinal axis.

Gain: (With respect to a linearly polarized isotropic reference antenna) -14 db at 36.44 MHz, -8 db at 72.88 MHz, and -4 db at 145.76 MHz.

Ground Antennas

Type: Crossed dipoles at all frequencies at Launch Site; crossed dipoles at 36.44 MHz and 72.88 MHz, helices at 145.76 MHz at Manolin Site.

Polarization: All frequencies had both right and left circular polarization at both sites.

Receivers

Launch Site: BRL-built combination receivers and phase locked tracking loops.

Manokin Site: BRL-built receivers and commercial tracking filters.

Resolution (AGC)

Launch Site: About ±1.5 db at all frequencies.

Manokin Site: About ±3.0 db at all frequencies.

cloud to an appropriately placed receiver (Figure 4). If the release cloud is or becomes ionized, the several frequencies will experience differing attenuations and differing phase path alterations. If the radio waves experience no angular refraction and the transmissions are phase coherent or extremely frequency-stable, the observed phase-path differences and signal attenuations can be simply related to total electron (or ion) content of the plasma cloud. In the more general case, and considering refraction and finite cloud sizes, the phase-path and attenuation observations must be combined in a fairly complex computer program to furnish both electron content and distribution, and then only if additional information on cloud size and location is available to initiate the computer routine.

Since a plasma is dispersive at radio frequencies, the terms dispersive phase and dispersive doppler are used in describing the real phase or frequency difference between differing frequency signals propagated through such a medium. Thus, in Figure 3, the quantity DD is the Dispersive Doppler; it is a frequency which is approximately proportional to the rate of change of integrated electron content along the low frequency ray path. The electron content may vary because of changes in ionization along the ray path, or motion of the rocket thru the ionization, or a combination of the two. If, in Figure 3, the observed dispersive doppler for 36.44 MHz and 145.76 MHz is designated $\Phi_{DD}(f_1,f_2)$ then,

$$\Phi_{DD}(f_1,f_2) = 2(4\phi_1 - \phi_2) \qquad (1)$$

since f_1 and f_2 are phase coherent. The quantities ϕ_1 and ϕ_2 are given by,

$$\phi_i = 2\pi f_i \int_0^s ds/c_i \qquad (2)$$

where, c_i = propagation velocity of the ith frequency and is dependent upon the location in space of the element of path length, ds. In the complexities of real life, the electron density is an implicit function of the propagation velocity and the propagation path depends upon the spatial distribution of electron density. Without some assumptions on

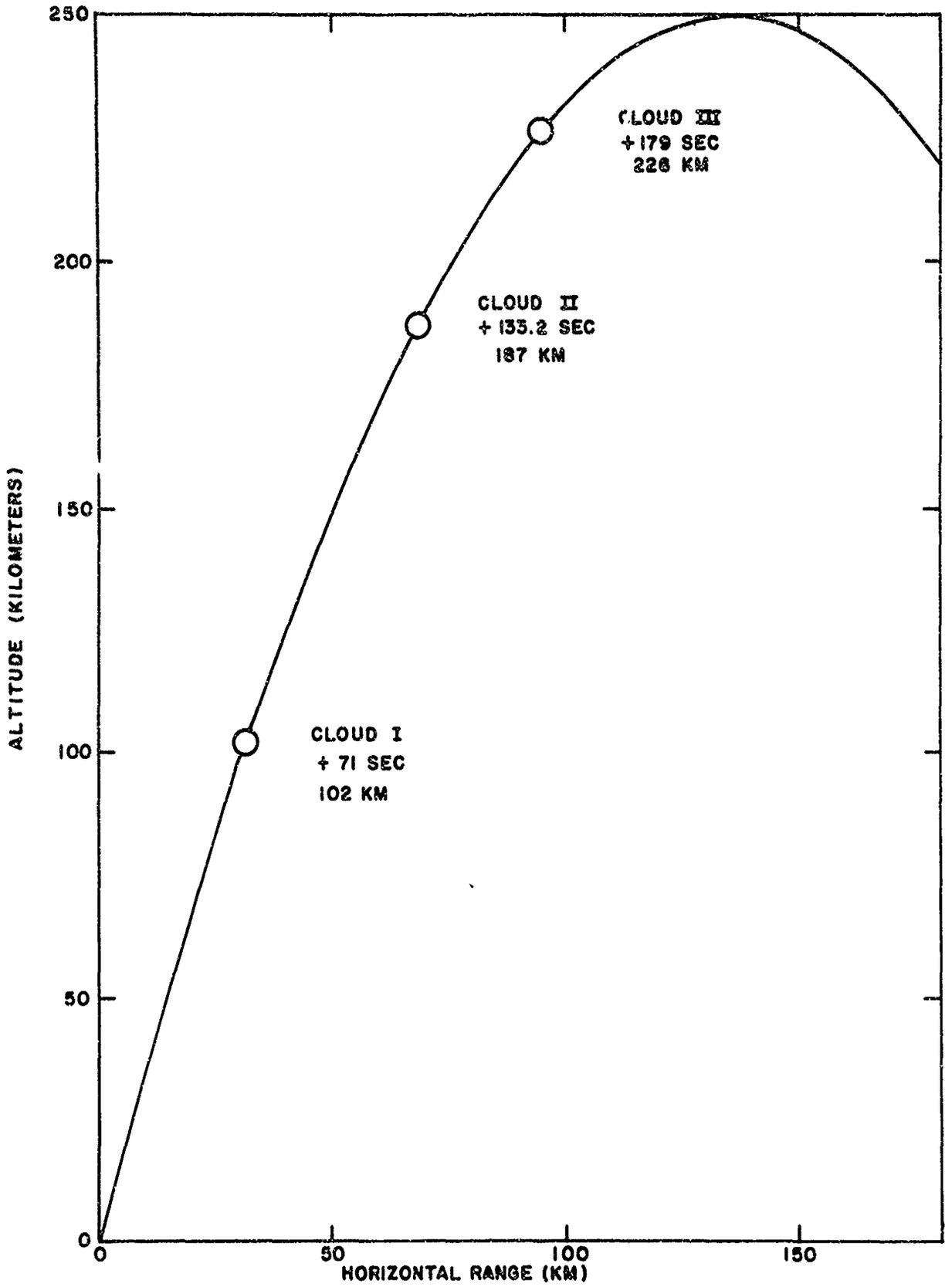

Figure 4. Elevation View of Rocket Trajectory.

the plasma distribution and/or a time function relationship for distribution changes, actual plasma electron densities cannot be derived from observations of Φ_{DD} or ϕ_i. However, if the transmitter and receiver are outside the plasma, a rather gross estimate of plasma location and distribution permits a determination of total electron content between transmitter and receiver using a "bootstrap" ray trace computer program. Recognizing that the Appleton-Hartree dispersion equation and a complete ray trace program (Davies 1965, Radio Science, 1968) are required for a general treatment, a simple expression for c_i in terms of electron density is possible on the assumption of a transmitting frequency large compared to either the plasma or electron gyromagnetic frequencies. Thus,

$$c_i = c_o/\mu = c_o\left[1 - \frac{e^2 N}{m\varepsilon_o \omega^2}\right]^{-\frac{1}{2}}$$

$$c_i \doteq c_o\left[1 - \frac{80.5N}{f_i^2}\right]^{-\frac{1}{2}} \doteq c_o\left[1 - \frac{40.3N}{f_i^2}\right]^{-1} \qquad (3)$$

where, N is the electron density, c_o is the vacuum velocity of propagation; μ is the index of refraction (real), e and m are the electron charge and mass respectively, ε_o is the free space permittivity, and ω is the propagating wave angular frequency. Assuming, further, that the phase paths at f_1 and f_2 are identical, substitution of Equations (3) and (2) into (1) gives,

$$\Phi_{DD} \doteq \frac{80.5(K^2-1)}{Kc_o f_1} \int_o^s N ds \qquad (4)$$

where, $K=f_2/f_1$. Again it is emphasized that in a real experiment employing two frequencies, the measured Φ_{DD} is not unambiguously related to $\int N ds$ as in Equation (4); however, employment of additional coherent transmissions and signal attenuation measurements can significantly reduce the ambiguity.

The radiowave absorption, per unit path, is given by the expressions (Davies 1965, 81-82):

Non Deviative:

$$\kappa_i = (e^2 \nu N)(8\pi^2 \varepsilon_o m c f_i^2)^{-1} \qquad (5)$$

Deviative:

$$\kappa_i = (e^2\nu N)[8\pi^2\varepsilon_o mcf_i^2(1-e^2N/4\pi^2 m\varepsilon_o f_i^2)^{\frac{1}{2}}]^{-1} \qquad (6)$$

for f_i much greater than the collision (ν) and electron gyromagnetic frequencies, and where κ_i is the absorption in nepers $(8.69db)m^{-1}$. In the propagation experiments here discussed, electron-neutral and electron-ion collisions must be considered in application of Equations (5) and (6). At the altitudes of interest here, absorption becomes significant only near the plasma frequency and, hence, is not a sensitive indicator of electron density at other than the plasma frequency.

As noted above, interpretation of the multifrequency propagation measurements in terms of electron content/electron density requires application of a ray trace program and some assumptions on the location and electron distribution for the chemical release plasma. A discussion of the ray-trace program is given in Appendix I; distribution and location assumptions are discussed in later paragraphs. Defocussing of the radio signals by the relatively small release plasma is significant and the effect must be considered in interpretation of the attenuation measurements.

III. FLIGHT SUMMARY

As indicated earlier, propagation data were obtained only for the second of the two rocket probes launched. Trajectory characteristics are shown in Figures 4 and 5 and the release parameters in Table II (Best, 1968; Noel, 1968). Performance of the vehicle, release locations and chemical yields were as predicted. The propagation experiment functioned properly with adequate signals received at the ground station located near the launcher. Signals at the remote receiver (Manokin Site) were lost from the time of second release to shortly before rocket apogee. The third release produced loss of signal phase lock for perhaps 3 seconds at the launcher receiver site and initiated rocket tumble.

IV. DATA

The processed data from the propagation experiment are the dispersive

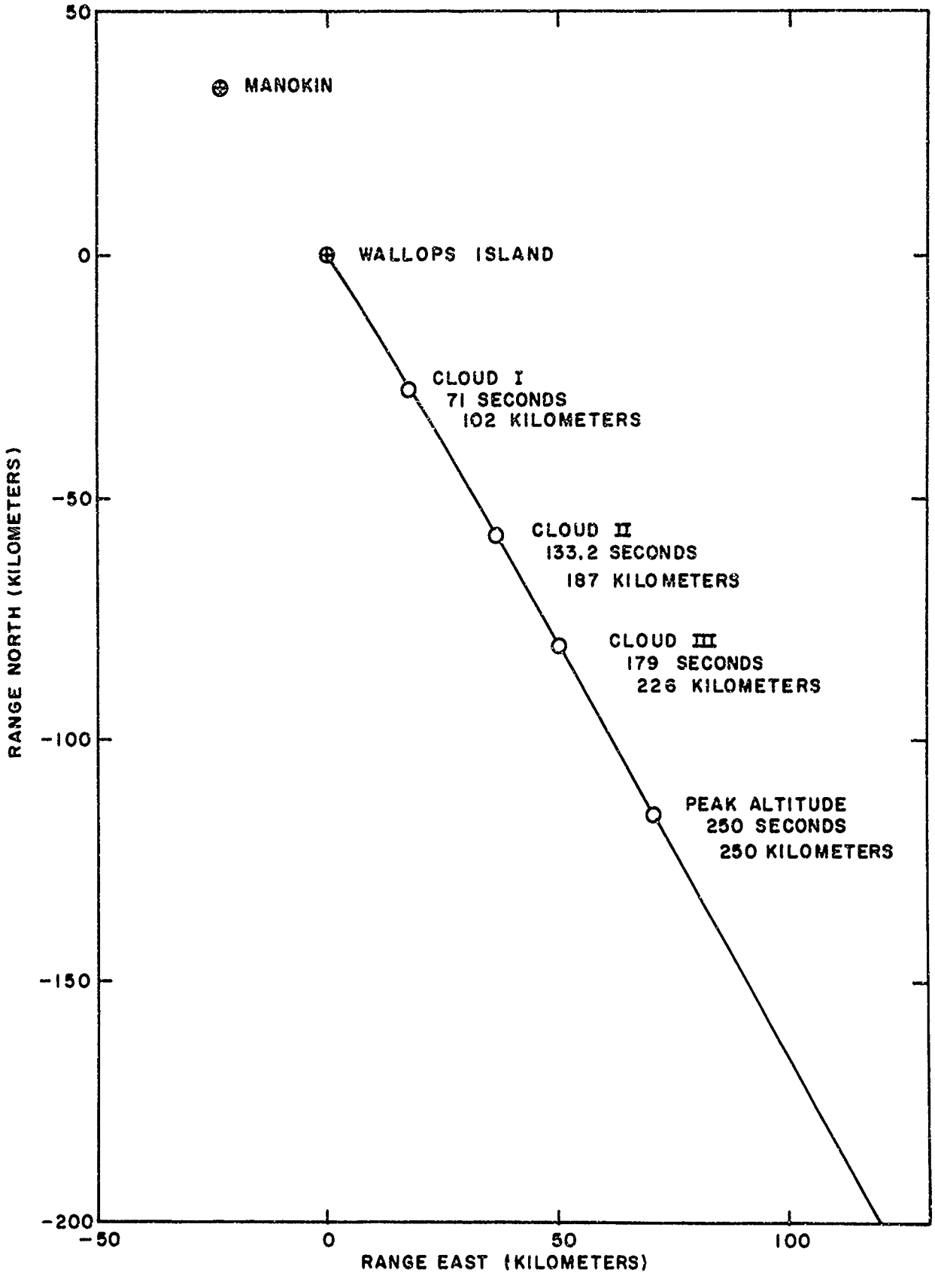

Figure 5. Plan View of Rocket Trajectory.

TABLE II. Chemical Release Parameters, Flight VERA (Oct. 4, 1967)

Release Event	Time (U.T.)	Lat. (N)	Long (W)	Alt. (KM)	Chemical* Payload	Vaporizable Barium (Mole)†	Solar** Horizon
I	2319:11	37.60°	75.29°	102.9	A	14	72
II	2320:13	37.34°	75.08°	186.9	A	14	78
III	2320:58	37.13°	74.94°	224.2	B	11.8	83

Notes:

*Payload A: 6kg(25% CuO, 75% Ba)

Payload B: 6kg(8% Be, 67% CuO, 27% Ba)

**Solar Horizon: Kilometers above sub-release point at time of release.

†Maxium barium available for vaporization following complete chemical reaction.

phase differences derived from suitable mixing of the 36.44-145.76 MHz signals (ϕ_{DD} of Equation 1), and signal strengths for the three propagated frequencies as measured at the receiving sites. For the sake of brevity, the beacon frequencies will hereafter be referred to as 36, 73, and 146 MHz. Two receiving sites were used, one at the launch site and the other near the town of Manokin, about 35 kilometers north and 23 kilometers west of the launch site. The dispersive phase (integrated dispersive doppler) measured at the Manokin site is shown in Figure 6. At the time of release of the second cloud (133.2 seconds) the signal strength dropped so that the tracking filters required for dispersive doppler measurements lost lock. The signal could not be reacquired until 225 seconds, shortly before peak altitude. Continuous data were obtained for the remainder of the flight.

Dispersive phase from launch site is shown in Figure 7. Continuous data were obtained throughout the entire flight except for a period of about three seconds following the third releae. The dotted line is the dispersive phase that would have been observed had the rocket been flown into an undisturbed ionosphere with the same profile as that computed from the downleg data (see below). The difference between the dotted curve and that for the actual data can therefore be attributed to the effect of the barium clouds. It is evident that the first cloud (71 seconds) produced no measurable dispersive doppler while the second and third events (133.2 and 179.0 seconds, respectively) produced marked dispersive phase. Effects due to the clouds ended at about 225 seconds and the dispersive phase due to the undisturbed ionosphere was measured for the remainder of the flight. An unusual feature of the launch site data is the large discontinuity in dispersive phase which appears to occur at the time of third release. Such a discontinuity has not been observed prior to this flight but it will later be shown that discontinuities can occur when multipath propagation is experienced. Further, it will be shown that the short section of seemingly inconsistent data between 174 and 179 seconds should not be plotted as shown. It should be replaced by a discontinuity at 174 seconds and be plotted slightly above the dotted line for the undisturbed ionosphere.

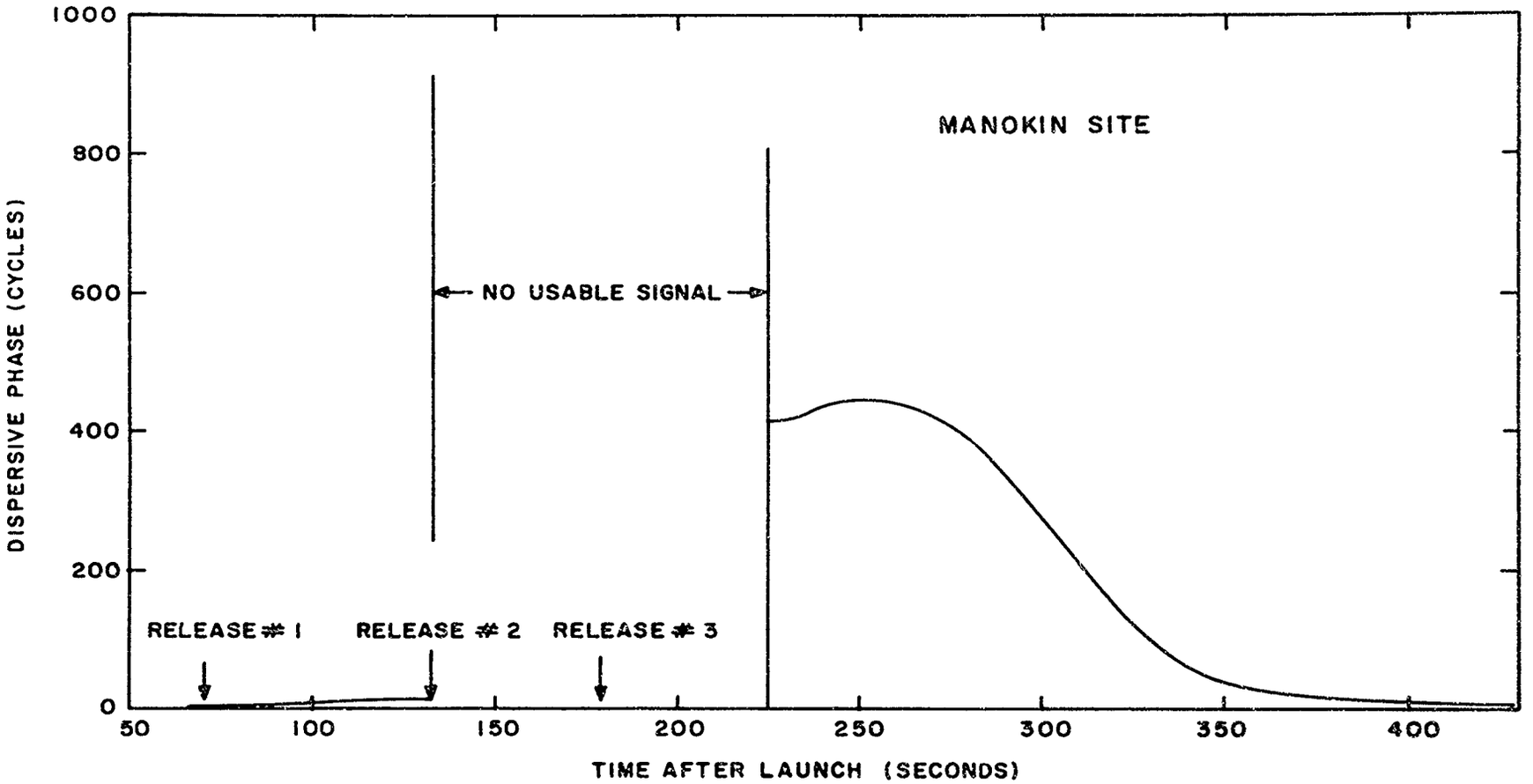

Figure 6. Manokin Site Dispersive Phase Vs Time.

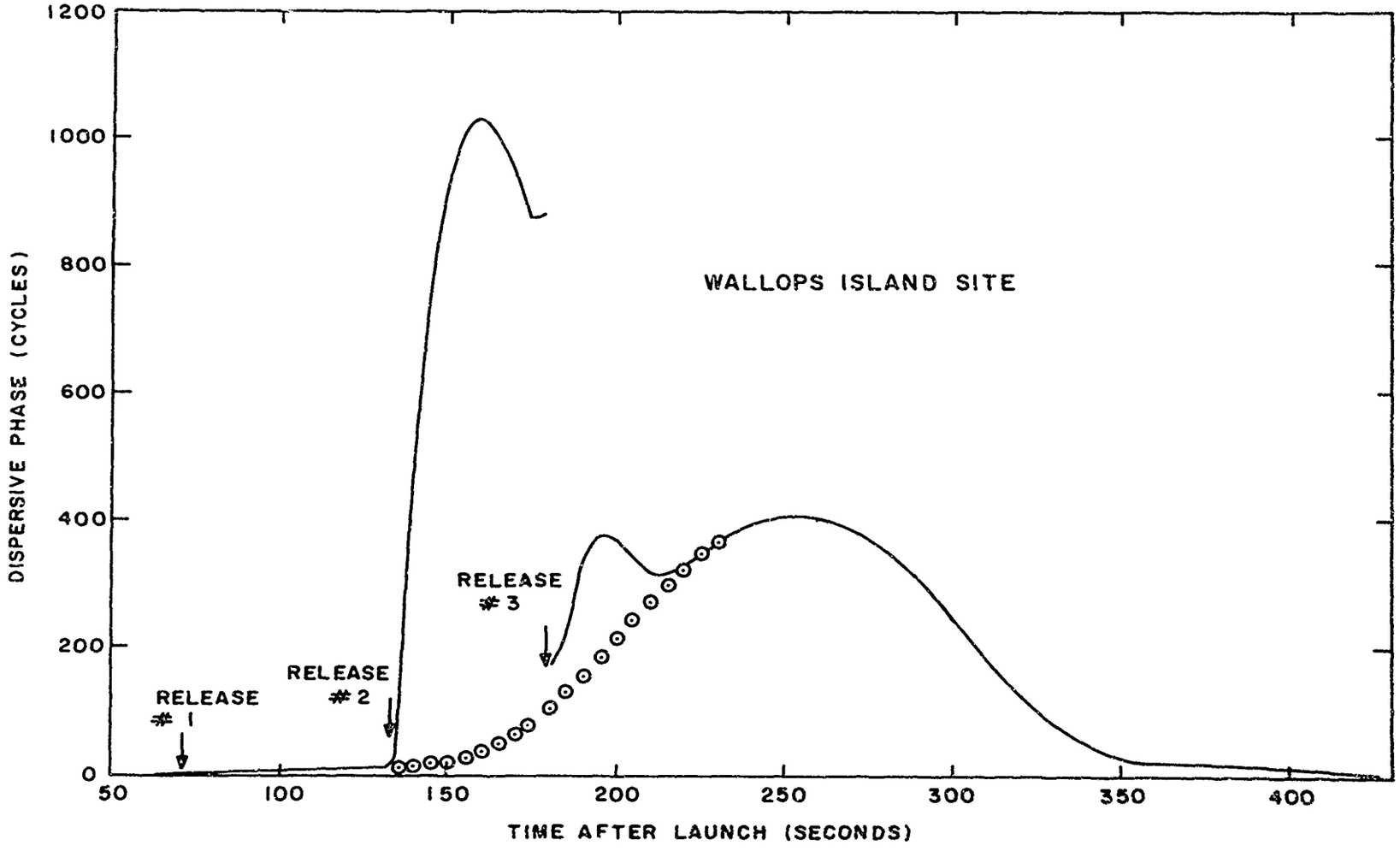

Figure-7. Launch Site Dispersive Phase Versus Time.

Figures 8 and 9 show the 36 MHz signal strength measured using the left-hand receiver AGC. There was a brief, sharp decrease in signal as a result of the first release at 72 seconds, after which the signal returned to approximately its undisturbed value. The signal dropout arises from a combination of two circumstances; early time thermal ionization in the thermite burning process (resulting in absorption), and strong defocusing by the localized electron cloud. The second release at 133.2 seconds caused a similar decrease which was followed by a couple of seconds of signal enhancement. The signal enhancement may result from focusing by the essentially neutral cloud existing immediately after exhaustion of the products from the canisters. The signal then decreased, with superimposed oscillations, until 174 seconds when it rapidly increased to another period of signal enhancement until the third release at 179 seconds. The third release caused another brief, sharp decrease in signal strength after which the signal only partially recovered to an essentially constant value, with superimposed fading for the remainder of the flight. Figure 10 shows the signal strength measured using the tracking filter AGC for comparison with Figure 9.

Figures 11 and 12 show the 73 MHz signal strength measured using the left-hand receiver AGC. The data are qualitatively similar to the 36 MHz data except that the fading oscillations after second release are more rapid and the sudden increase in signal strength prior to third release occurs earlier, at 166.7 seconds. The oscillations or "beats" which are quite noticeable at 36 and 73 MHz from 140 to 160 seconds (from 7 to 27 seconds after release) possibly arise from a dense core of ionization or an ionization front advancing from the sunlit side of the cloud. The apparent integral relation of the beat periods of the two frequencies suggests this interpretation.

Figures 13 and 14 show the 146 MHz signal strength measured using the left-hand receiver AGC. The major difference, compared to the lower frequencies, occurs between the second and third releases. After the initial dropout there is a gradual decrease and recovery without the fading that is characteristic of the lower frequencies. There is also no

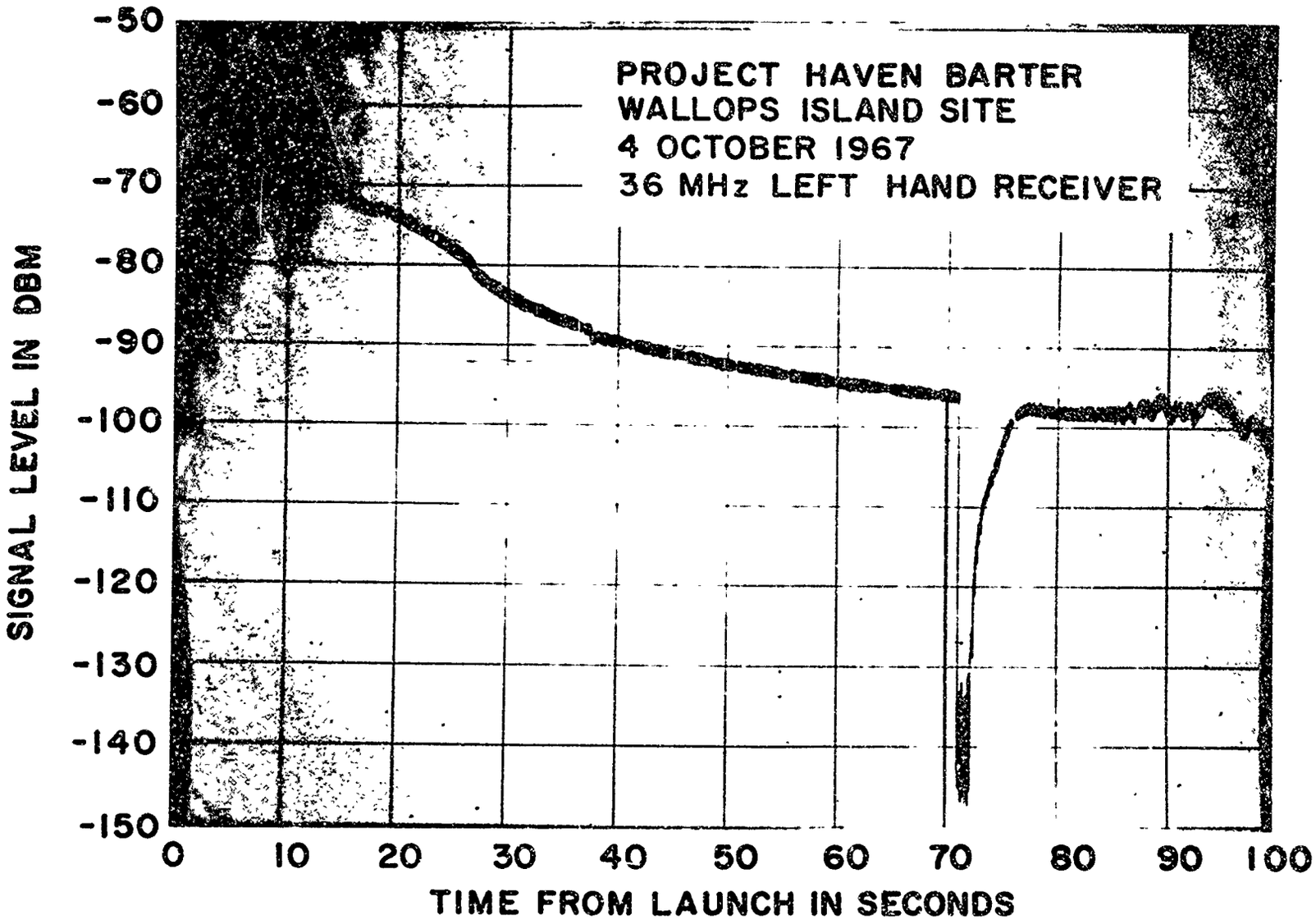

Figure 8. Signal Strength at 36.44 MHz (Receiver AGC), 0-100 Seconds.

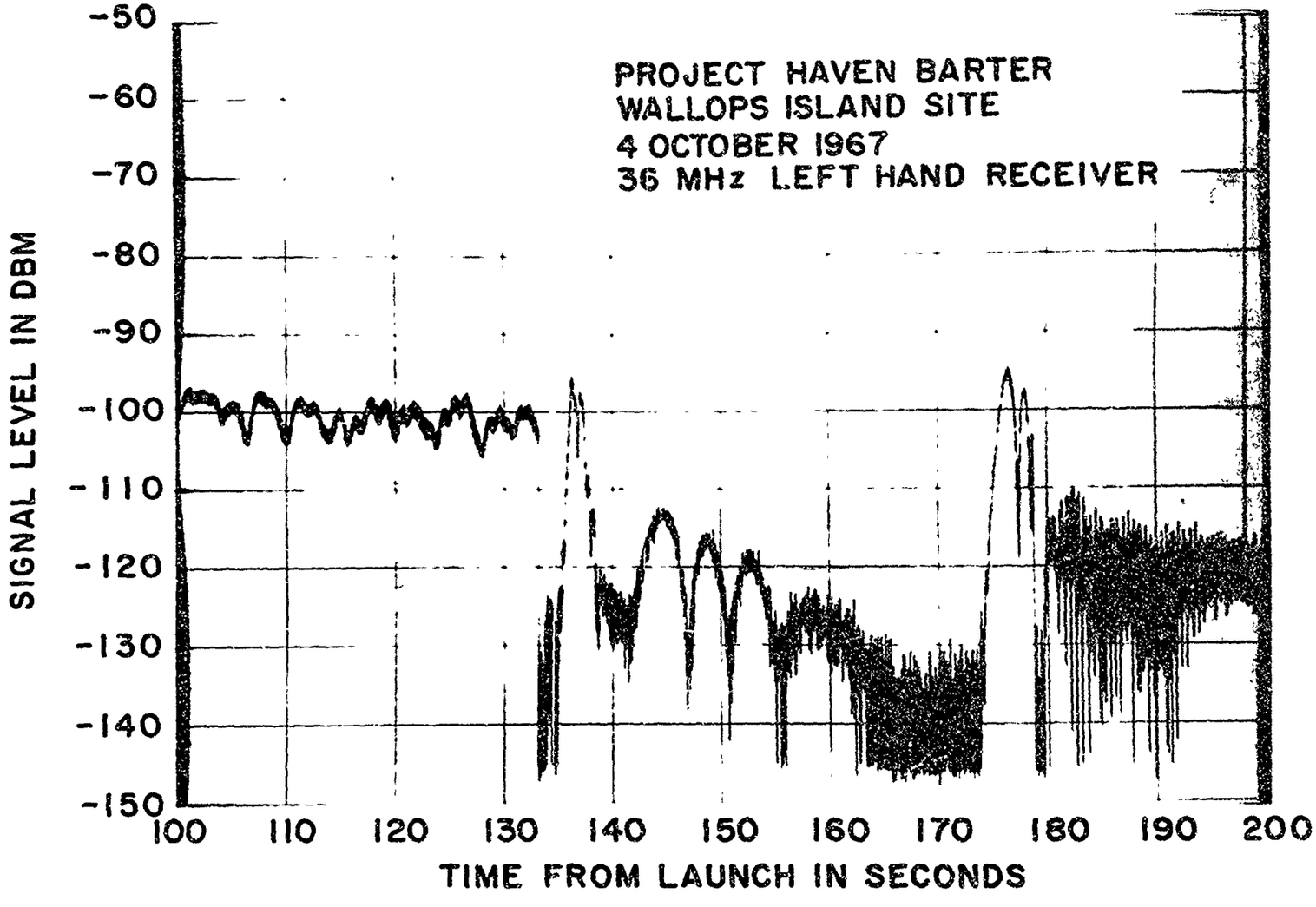

Figure 9. Signal Strength at 36.44 MHz (Receiver AGC), 100-200 Seconds.

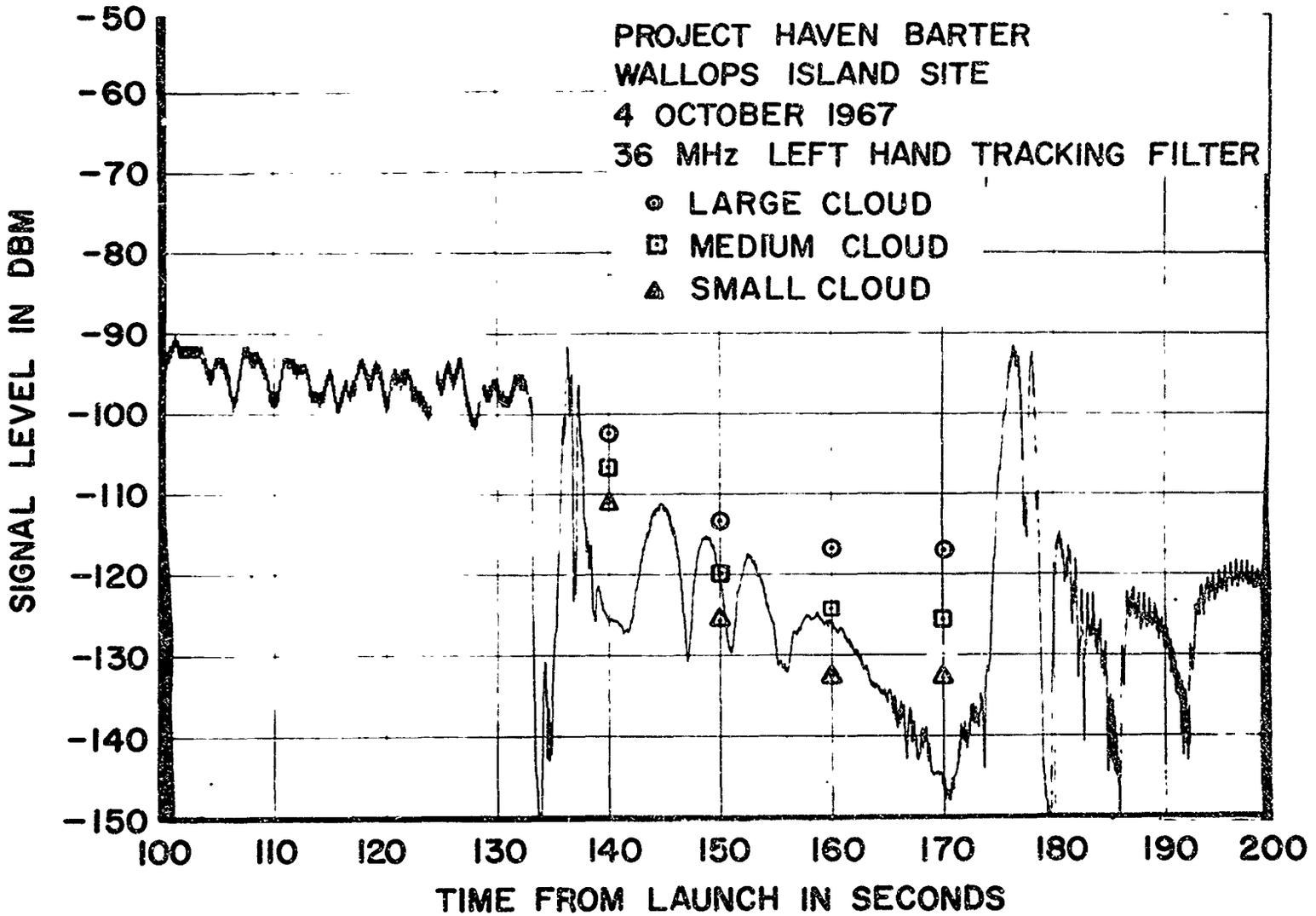

Figure 10. Signal Strength at 36.44 MHz (Tracking Filter AGC), 100-200 Seconds.

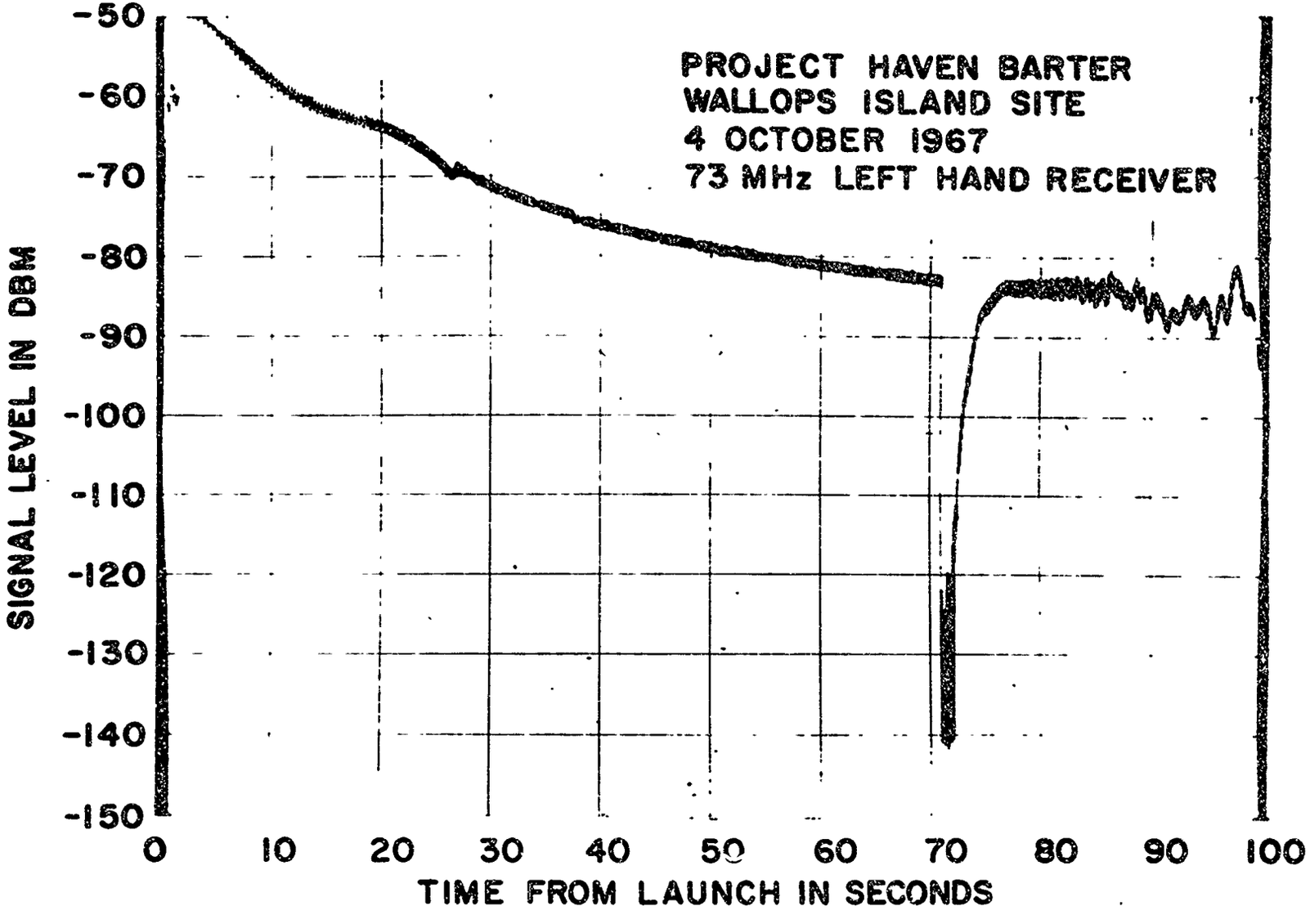

Figure 11. Signal Strength at 72.88 MHz (Receiver AGC), 0-100 Seconds.

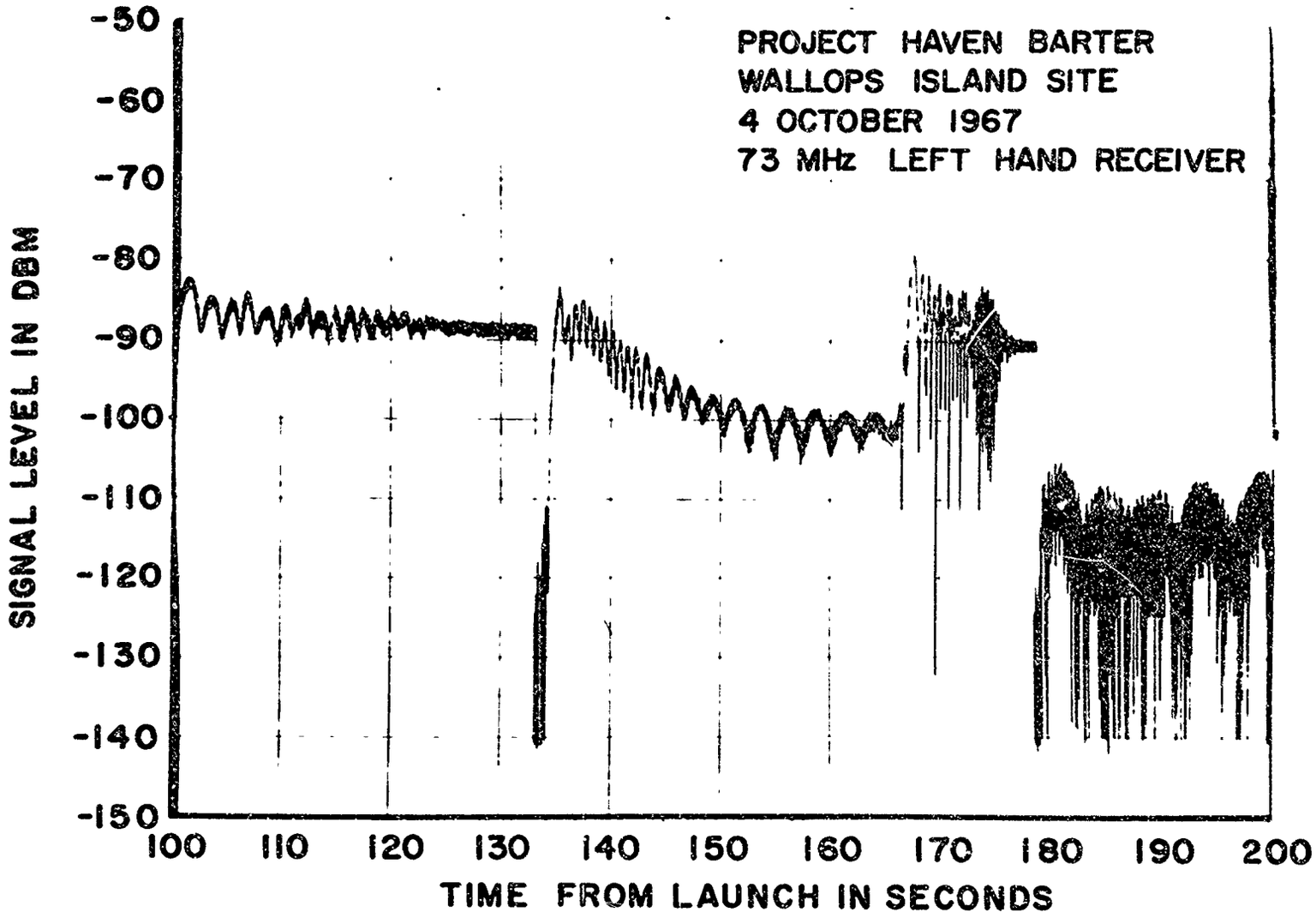

Figure 12. Signal Strength at 72.88 MHz (Receiver AGC), 100-200 Seconds.

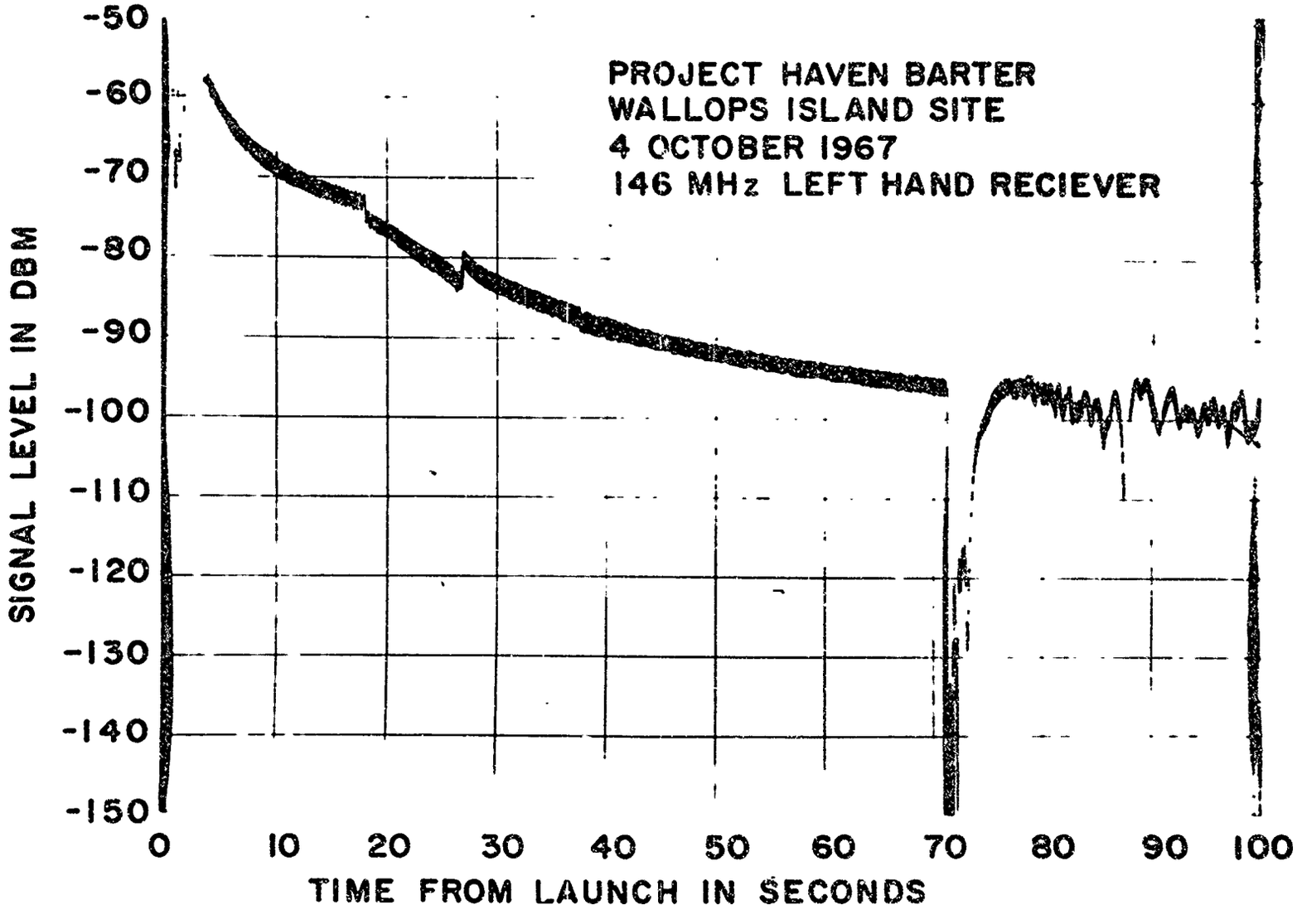

Figure 13. Signal Strength at 145.76 MHz (Receiver AGC), 0-100 Seconds.

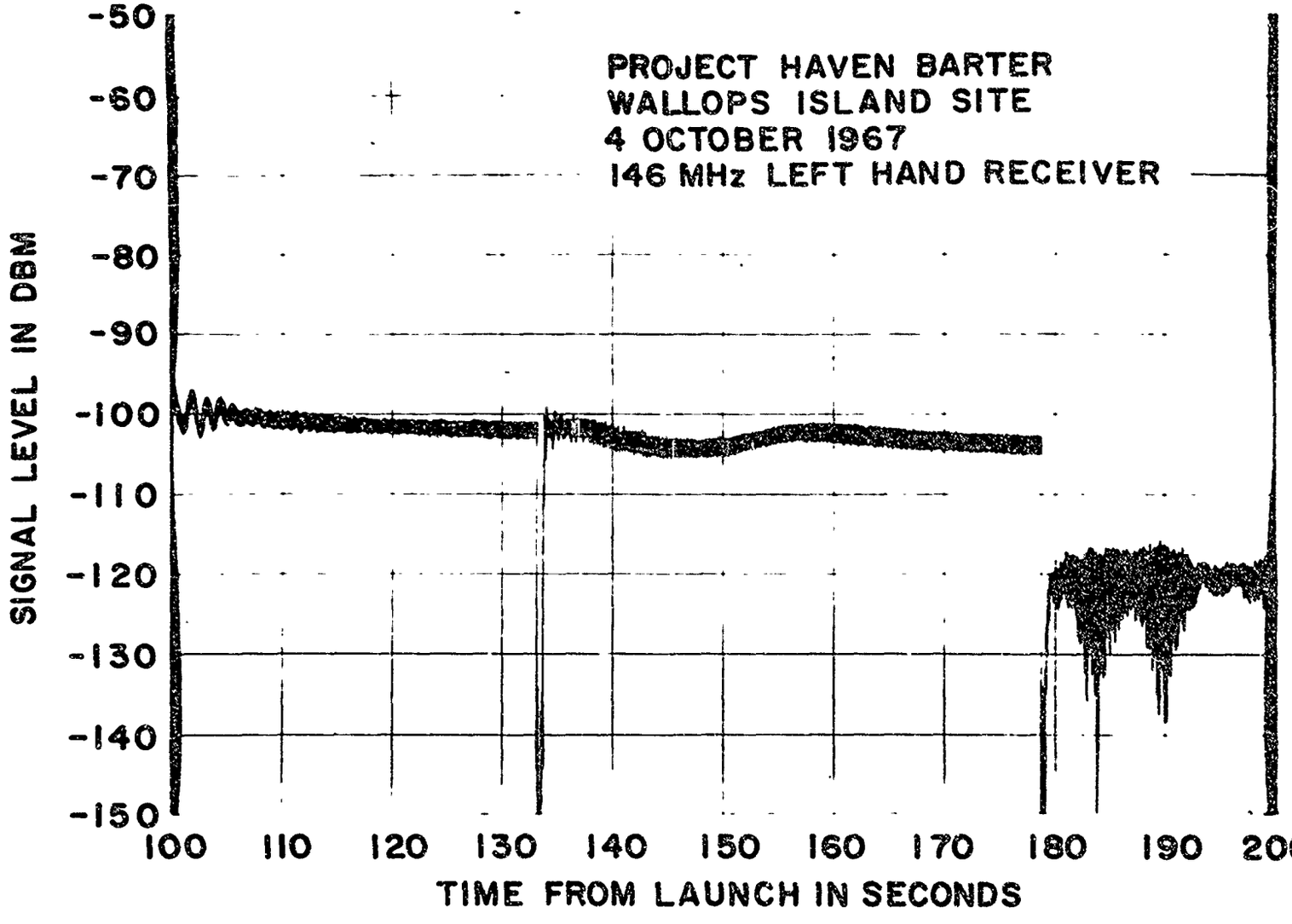

Figure 14. Signal Strength at 145.76 MHz (Receiver AGC), 100-200 Seconds

sudden increase in signal strength prior to third release.

V. ANALYSIS

The computation of electron density profiles from dispersive phase normally assumes either a horizontally stratified, time invarient ionosphere or one that can be effectively reduced to that case. For this experimental technique the method for computing electron density profiles has been described (Dean and Lootens, 1968). The effect of horizontal gradients and temporal variations has been discussed (Lootens and Prenatt, 1967).

The VERA flight was the first for which two separated receiving stations were employed. As a result, the flight provided a limited test of the validity of the "standard" computational technique. Figure 15 shows the electron density profiles computed using the downleg data from the two receiving sites. Also shown is the profile computed from a sweep frequency ionosonde located near the launch site (Wright and Paul, 1967).

A qualitative interpretation of a number of features of the dispersive doppler and signal strength data obtained during rocket ascent can be given with the aid of Figure 16. The cloud, with an index of refraction of less than unity, acts as a diverging lens. Rays passing through the cloud are diffused over a rather wide area; measured signal levels at the ground would accordingly be reduced. The prolonged increase in observed dispersive phase for the second cloud results from the fact that the rays arriving at the receiver continue to pass near the center of the cloud even though the rocket itself is emerging from behind the cloud. Three regions have been labeled in Fig. 16; indirect, multipath, and direct. In the indirect region, only rays that have passed close to the center of the cloud are received (the indirect rays). In the direct region only rays which have been little affected by the cloud are received (the direct rays). In the multipath region both direct and indirect rays reach the receiver. As the rocket moves upward and to the right, the inside edge of the multipath region moves to the left so that, if a multipath region exists at all, there occurs a time for a given location when

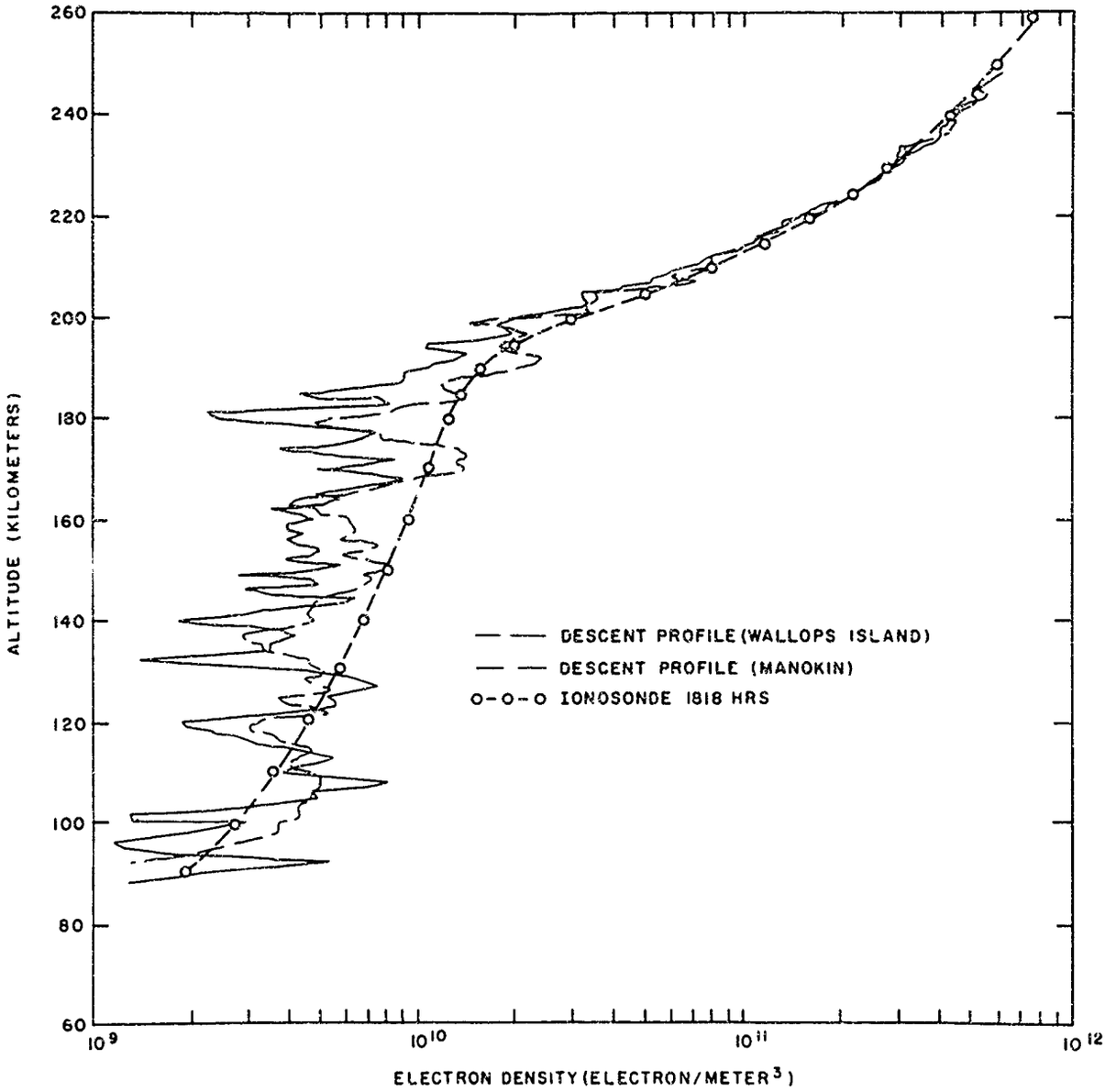

Figure 15 Electron Density Profiles, Rocket Flight Vera

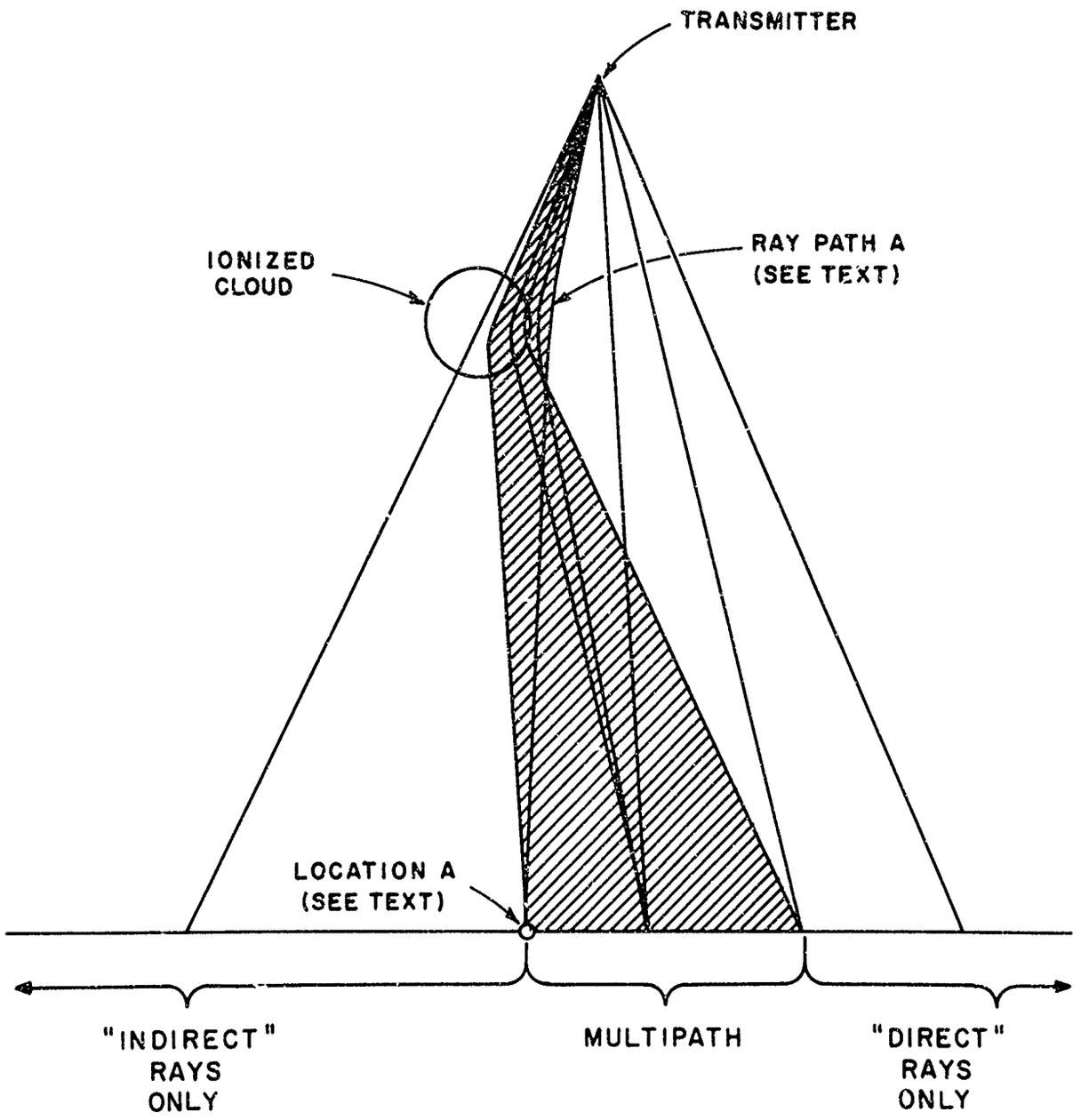

Figure 16. Sketch Illustrating The Effect of an Ionized. Cloud on Propagation Paths.

the direct signal is first received. At that time for a receiver position corresponding to "Location A" in Figure 16, some focusing of the rays occurs at the inner edge of the multipath region leading to signal enhancement. The "earliest multipath" effect can explain both the sudden increases in signal strength at 36 and 73 MHz and the sudden change in slope of the dispersive phase at 174 seconds. At that itme, the 36 MHz phase-locked tracking filters lost the weak indirect signal and locked onto the much stronger direct signal (labeled "Ray Path A" in Figure 16). From Figure 16 it is evident that between 174 and 179 seconds the measured dispersive phase is along the direct ray path which is relatively little affected by the cloud. As a result, the dispersive phase during that period should not be plotted as shown in Figure 7, but should appear slightly above, and approaching, the dotted line corresponding to the undisturbed ionosphere.

Following the third release, the absence of effects characteristic of "earliest multipath" indicates that multipath was not observed for that cloud.

A preliminary quantitative interpretation of the dispersive doppler and signal strength data has been attempted while the signal was being affected by the second barium cloud. A spherically sysmmetric cloud model, whose defining parameters are shown in Figure 17, was postulated. The electron density was assumed to be gaussian with a total electron inventory beginning at zero and asymptotically approaching some limiting value. The square of the gaussian scale radius was assumed to increase linearly from some initial value as the cloud grew by diffusion. Ion cloud drift was determined from optical data (Noel, 1968). A ray tracing program (see Appendix I) was employed to compute the dispersive phase corresponding to the cloud models. The parameters defining the cloud were adjusted until agreement was achieved between computed dispersive phase and that actually measured.

Two approaches were used adjusting cloud parameters. One involved adjusting the ionization time constant, τ, the total inventory limit TI_{lim}, the initial scale radius, h_{g_o}, and the cloud growth rate, $\frac{dh_g}{dt}(=4D)$,

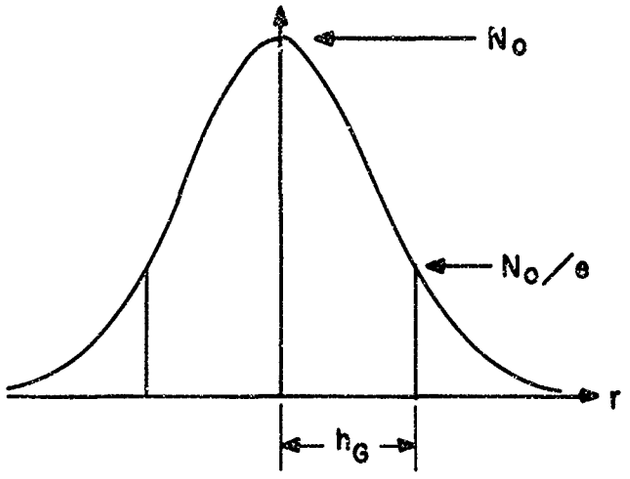

GAUSSIAN CLOUD

$$N = N_0 e^{-r^2/h_G^2}$$

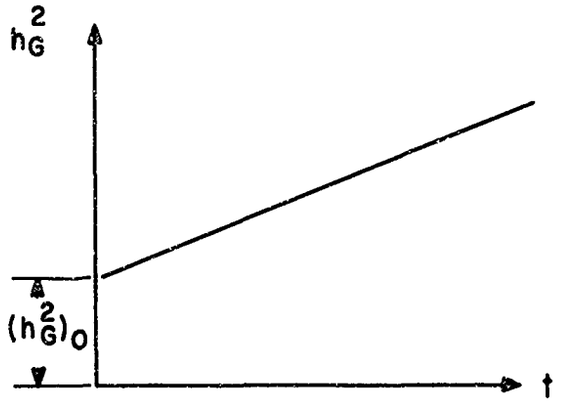

SCALE RADIUS

$$h_G^2 = (h_G^2)_0 + 4Dt$$

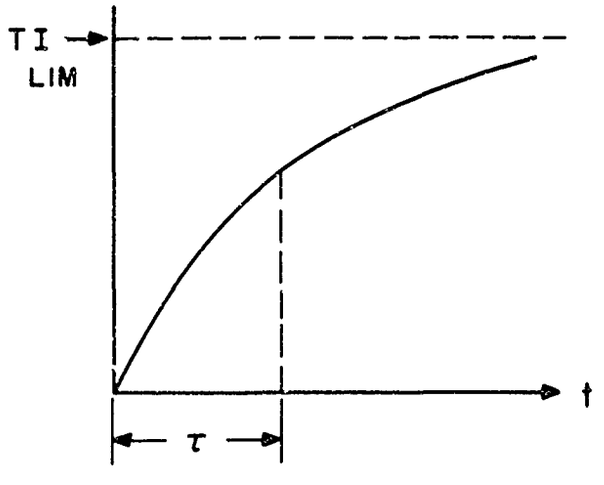

TOTAL INVENTORY

$$TI = TI_{LIM}(1 - e^{t/\tau})$$

$$TI = \pi^{3/2} N_0 h_G^3$$

Figure 17. Parameters Defining Spherically Symmetric Gaussian Clouds.

to bring the computed and measured dispersive phase into agreement. Using this approach, three clouds were defined, each of which reproduced the measured dispersive phase to within 1-2 percent between 140 and 174 seconds. The several cloud models, in terms of scale radius and total ion inventory, are shown in Figure 18, where the crosses connected by dashed lines indicate cloud parameters at several times following release (release occurred at 133.2 seconds). The defining cloud parameters are listed in Table III.

The other approach in determining cloud parameters considered only scale radius and total inventory. A value of scale radius was selected and the values of total inventory that would reproduce the data were computed for several times. This approach resulted, for cloud II, in the family of nearly straight lines, each for a different time, shown in Figure 18.

Based on dispersive phase data alone, it was not possible to decide among the various cloud models, each of which reproduced the measured data. To resolve the ambiguity it was necessary to include analysis of the signal strength data. As discussed earlier, the large increases in the strength of the 36 and 73 MHz signals prior to third release were assumed to correspond to first arrival of the direct radio wave signal. Each of the clouds, defined in Table III, was considered at 174 seconds and families of 36 MHz rays were traced through each cloud. Plots of these ray traces are shown in Figure 19. The family of rays for the large cloud shows that, at 174 seconds, the inside edge of the multipath region had not yet reached the observer so the increase in signal strength would not have occurred as early as 174 seconds. The family of rays for the small cloud shows that multipath was already being experienced prior to 174 seconds. The family of rays for the medium cloud shows that the inside edge of the multipath is almost coincident with the observer.

The same exercise was carried out for the 73 MHz signal at 166.7 seconds. The results, shown in Figure 20, are essentially the same as for 36 MHz except that for the large cloud multipath is not even possible. As a result, it appears that the medium cloud exhibits the best agreement with the measured data.

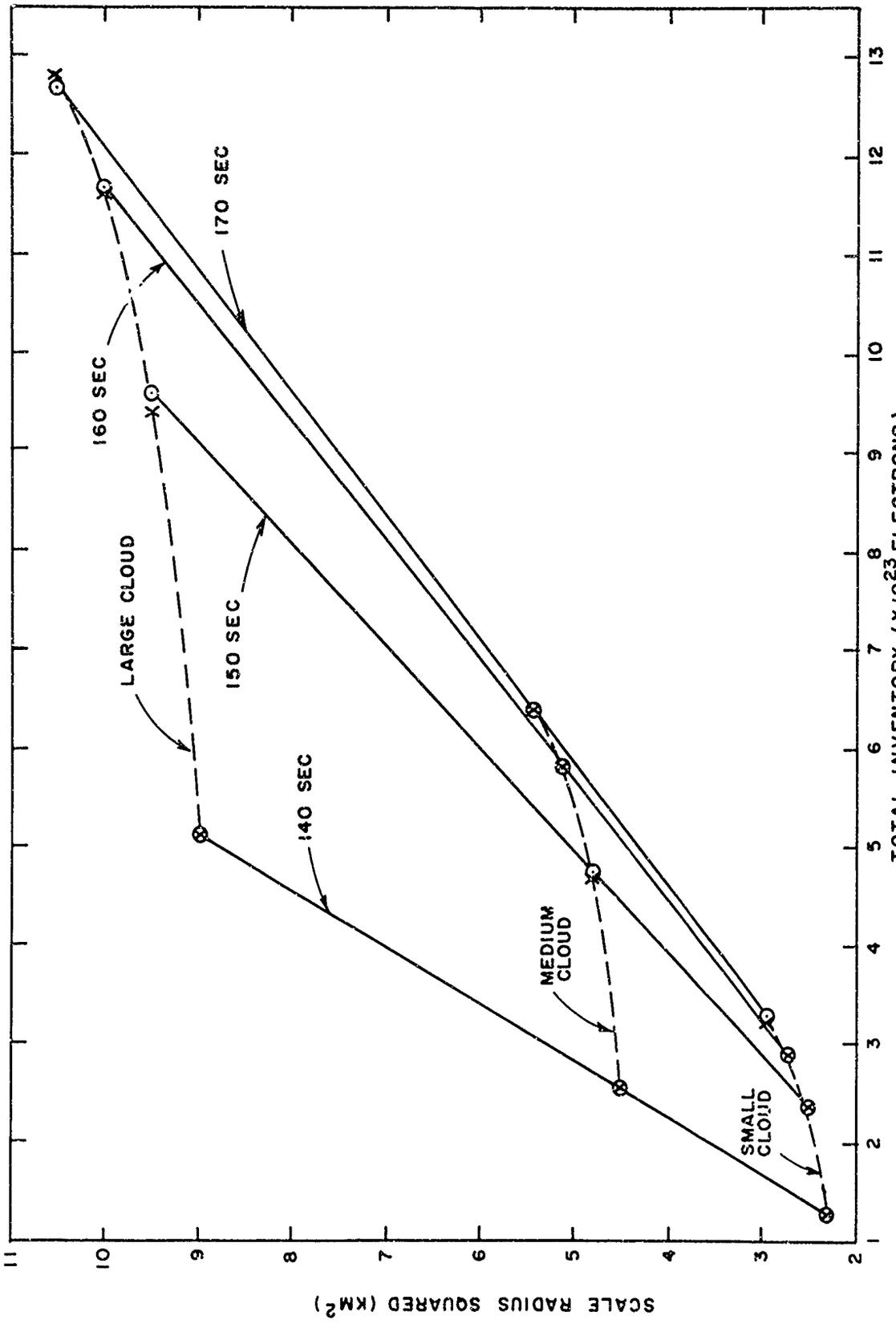

Figure 18. Cloud Parameters (Scale Radius Squared and Total Electron Inventory) Which Reproduce Measured Dispersive Phase.

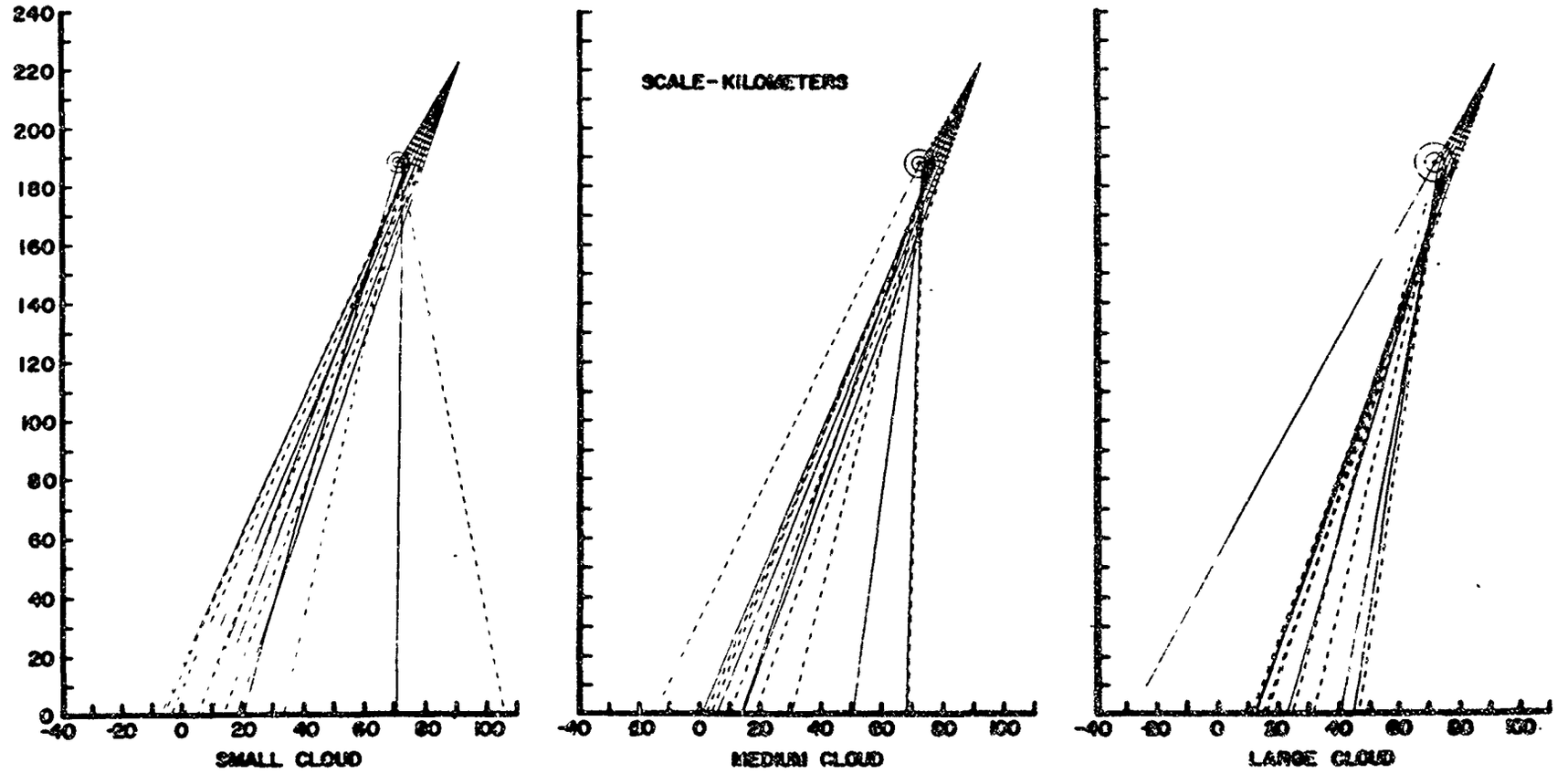

Figure 19 Raysets at 36.44 MHz for Three Model Clouds at 174.0 Seconds

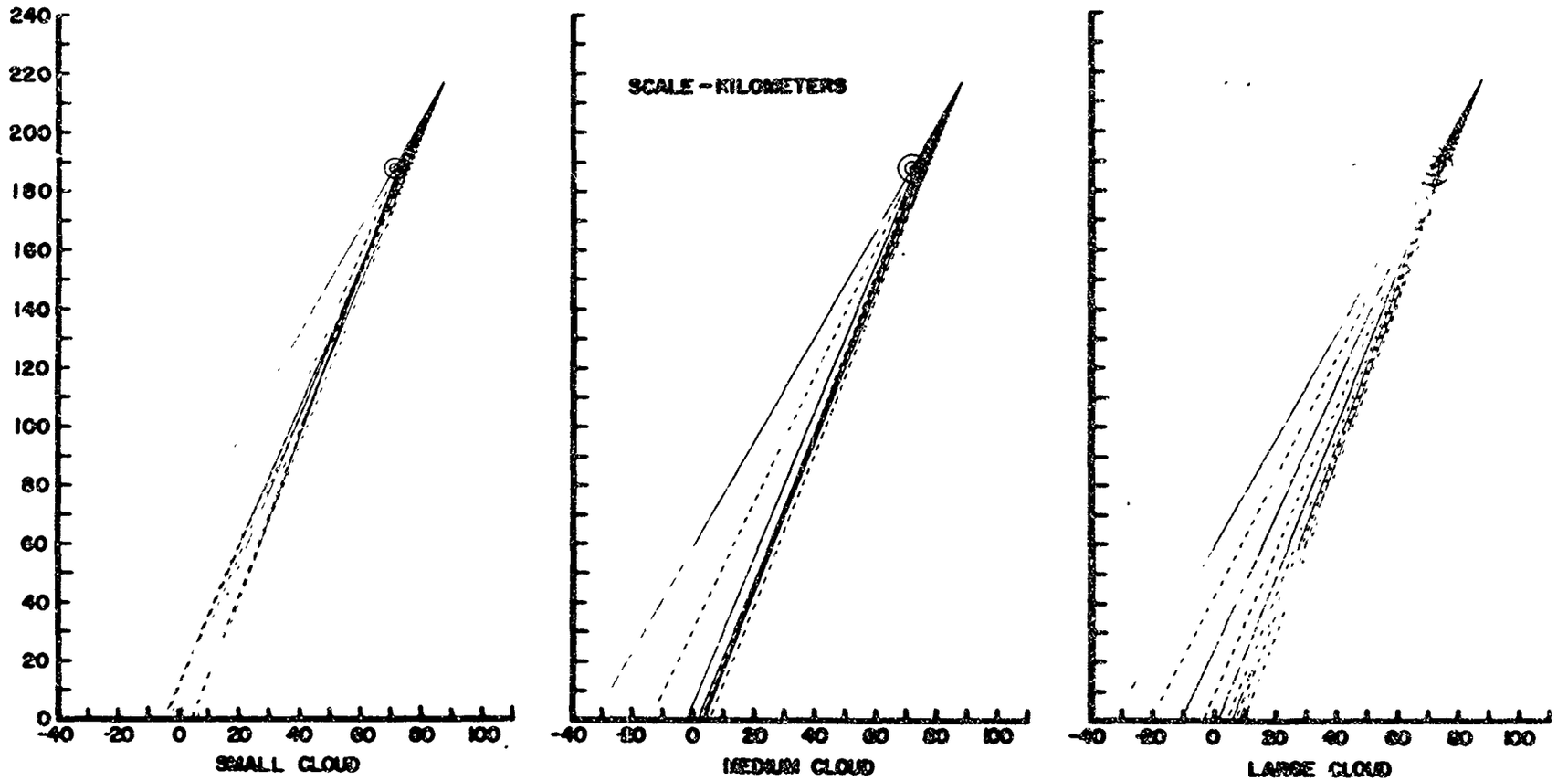

Figure 20 Raysets at 72.88 MHz for Three Model Clouds at 166.7 Seconds

TABLE III. Parameters Defining Cloud II Models That Reproduced Measured Data

	Large Cloud (C)	Medium Cloud (B)	Small Cloud (A)
Time Constnat (seconds)	15	15	15
Limiting Total Inventory (electrons)	1.4×10^{24}	7.0×10^{23}	3.5×10^{23}
Scale Radius Squared (km^2)	8.644 +.0510 (t-133.2)	4.298 +.0309(t-133.2)	2.166+.021(t-133.2)

By a technique briefly outlined in Appendix I, reductions of signal levels by the defocusing mechanism were computed at selected times for the several cloud models. Results of the computation are given in Table IV and, for the 36 MHz ordinary mode signals, are plotted in Figure 10. Comparison of the computed and measured signal strengths at 36 MHz would seem to indicate a cloud somewhat smaller than cloud model B and departing from spherical symmetry after 160 seconds.

An attempt was made to perform an analysis of the Cloud III data similar to that done for Cloud II. However, at the time of this writing, no satisfactory combination of parameters has been found for a sperically symmetric cloud that will reproduce the cloud. It appears that analysis of the Cloud III data will require use of a more elaborate model, for example a field-aligned, prolate spheriod. Current plans call for analysis of the data from both clouds using such a model.

VI. CONCLUSIONS

The preceeding sections describe a specific barium release ion cloud in terms of peak electron density, total ion inventory, ion diffusion rate and ion cloud radius for the interval $10<t<40$ seconds following release. The model for the cloud assumes a gaussian distribution for barium ions and diffusion radially symmetric in the time interval examined. The model parameters are forced to fit dispersive phase and signal strength data derived from a radio wave technique employing a multifrequency phase-coherent beacon transmitting through the ion cloud as it forms and grows.

For the release mixture given in Table I and deployed at 187 km., the release cloud characteristics may be summarized as follows:

Time Constant for Ba II formation --- 15 sec

Diffusion Coefficient for Ba II (approx. perpendicular to B) -- $7.5\text{x}10^{-3}\text{km}^2\text{sec}^{-1}$

Peak Electron Density (at release+38 sec) ----$9\text{x}10^6$el cm^{-3}

Total Ion Inventory (release+∞) -------- $7.0\text{x}10^{23}$

Scale Radius Perpendicular to $\vec{B}$ (release+40 sec) ---- 2.35 km

TABLE IV. Computed Signal Loss by the Defocusing Mechanism (36 MHz, Ordinary Mode)*

Time (after release) \ Cloud Model	Model A (Small)	Model B (Medium)	Model C (Large)
7 sec	-14.8±0.4 db	-9.5±0.3 db	-5.5±0.2 db
17	-29.5±0.5 db	-21.6±0.6 db	-14.7±0.5 db
27	-35±1.0 db (-12.9±0.7 db at 73 MHz)	-26.4±1.0 db (-8.3±0.6 db at 73 MHz)	-18.5±1.0 db (-4.9±0.5 db at 73 MHz)
37	-35.5±1.5 db	-28±1.2 db	-20.3±1.1 db

*Signal loss is approximately 5% greater for the extraordinary mode

The derived parameters of the barium cloud appear quite reasonable, although comparative optical data are very sparse at the early times at which the radio frequency measurements are made. The total ion inventory derived represents an ion yield of 2.6% of the total chemical payload mass. The diffusion coefficient appears low (approximately one-fifth the neutral barium atom diffusion coefficient at the release altitude) but is not unreasonable, since the coefficient measured represents diffusion normal to the magnetic field because of the geometry of release and the radio wave ray paths involved.

The technique of utilizing radio wave transmissions to describe barium cloud (or any plasma) properties has several domains of application. If ionization time constant and time for neutral cloud stabilization are short compared to the time the receiver site is eclipsed by the cloud, the technique is useful in describing initial cloud development, ion cloud diffusion, ion inventory, and peak cloud electron densities. If the transmissions through the cloud take place at late time (i.e., after the plasma cloud striates), the technique furnishes information on cloud structure, signal defocusing and on electron densities if a reasonable cloud model can be postulated.

Perhaps the most interesting result of the specific experiment discussed here is the strong defocusing of the radio signals as evidenced in Figures 10, 12, and 14. The signal attenuation is entirely the result of the defocusing mechanism; absorption plays no part at the altitude of release. Under circumstances for which the transmitter is far removed from the plasma cloud, the affected area on the ground would be restricted to the size of the eclipsing plasma. For transmissions from the ground, defocusing effects would be widespread for transmitter-receiver distances large compared to the transmitter-cloud distance.

Considerably more analysis is required to understand the details (periodic fading) in the signal strength data.

REFERENCES

1. D. R. Bates, "A Suggestion Regarding the Use of Rockets to Vary the Amount of Atmospheric Sodium," J. Geophs. Res., Vol 55, 1950, pp. 347-349.

2. G. T. Best, Air Force Cambridge Research Laboratories, Private Communication, 1968.

3. K. Davies, Ionospheric Radio Propagation, National Bureau of Standards Monograph 80, 1965, p.73ff.

4. W. A. Dean, and H. T. Lootens, "Ionosphere Measurements with a Four-Frequency, Phase Coherent Beacon," Ballistic Research Laboratories Report No. 1396, March 1968.

5. G. A. Dulk, and W. A. Dean, "Rocket and Satellite Studies Using a Digital Ray Tracing Proceedure: Summary Report," Ballistic Research Laboratories Report No. 1163, December 1962.

6. H. Föppl, G. Haerendel, L. Haser, J. Loidl, P. Lütjens, R. Lüst, F. Melzner, B. Meyer, H. Neuss, and E. Rieger, "Artificial Strontium and Barium Clouds in the Upper Atmosphere," Planet. Space Sci., Vol 15, 1967, pp. 357-372.

7. G. Haerendel, and R. Lüst, "Artificial Plasma Clouds in Space," Scientific American, Vol 219, November 1968a, pp. 80-92.

8. G. Haerendel, and R. Lüst, "Electric Fields in the Upper Atmosphere," Earth's Particles and Fields, B. M. McCormac, Editor, New York, Reinhold Book Corp., 1968b, pp. 271-285.

9. J. Hazelgrove, "Ray Theory and a New Method for Ray Tracing," Report of Conference on Physics of the Ionosphere, The Physical Society, London, 1955, p. 355.

10. R. M. Jones, "A Three-Dimensional Ray Tracing Computer Program," ESSA Technical Report IER 17-ITSA17, December 1966.

11. R. S. Lawrence, and D. J. Posakony, "A Digital Ray Tracing Program for Ionosphere Research," Proceedings of the Second International Space Science Symposium, Florence, April 10 - 14, 1961, Amsterdam, North Holland Publishing Company, 1961.

12. K. H. Lloyd and L. M. Sheppard, "Atmospheric Structure at 130-200 km Altitude from Observations of Grenade Glow Clouds during 1962-63," Australian Journal of Physics, Vol 19, 1966, pp. 323-342.

13. H. T. Lootens and R. E. Prenatt, "Re-Evaluation of Fish Bowl Project 6.3 Electron Density Profiles," Ballistic Research Laboratories Memorandum Report No. 1865, July 1967.

14. T. M. Noel, Air Force Cambridge Research Laboratories, Private Communication, 1968.

15. Radio Science, "Special Issue on Ray Tracing," Vol 3, No.1, 1968.

16. N. W. Rosenberg, "Chemical Releases at High Altitudes," Science, Vol 152, 20 May 1966, pp. 1017-1027.

17. N. W. Rosenberg and D. Golomb, "Generation and Properties of High Altitude Chemical Plasma Clouds," Ionization in High Temperature Gasses, Progress in Astronautics and Aeronautics, Vol 12, K. Shuler, Editor, Academic Press, 1963, pp. 395-408.

18. J. W. Wright and A. K. Paul, "Some Preliminary Results and Interpretation of Ionosonde Observation of Barium Ion Clouds," ITSA, Boulder, Colorado, Unpublished Memorandum.

APPENDIX I: RESUME OF THE RAY TRACE PROGRAM

The ray tracing program used here is a combination of two earlier programs. The actual stepping of the ray is accomplished by numerical integration of a set of differential equations similar to Hazelgrove's equations (Hazelgrove, 1954; Jones, 1966). The equations are:

$$\frac{dr}{dt} = \frac{1}{\mu} \left(V_r - \mu \frac{\partial \mu}{\partial V_r}\right)$$

$$\frac{d\theta}{dt} = \frac{1}{\mu\mu' r} \left(V_\theta - \mu \frac{\partial \mu}{\partial V_\theta}\right)$$

$$\frac{d\phi}{dt} = \frac{1}{\mu\mu' r \sin\theta} \left(V_\phi - \mu \frac{\partial \mu}{\partial V_\phi}\right)$$

$$\frac{dV_r}{dt} = \frac{1}{\mu'} \frac{\partial \mu}{\partial r} + V_\theta \frac{d\theta}{dt} + V_\phi \sin\theta \frac{d\phi}{dt}$$

$$\frac{dV_\theta}{dt} = \frac{1}{r} \left(\frac{1}{\mu'} \frac{\partial \mu}{\partial \theta} - V_\theta \frac{dr}{dt} + rV_\phi \cos\theta \frac{d\phi}{dt}\right)$$

$$\frac{dV_\phi}{dt} = \frac{1}{r \sin\theta} \left(\frac{1}{\mu'} \frac{\partial \mu}{\partial \phi} - V_\phi \sin\theta \frac{dr}{dt} - rV_\phi \cos\theta \frac{d\theta}{dt}\right)$$

where r, θ, and ϕ are the spherical coordinates of a point on the ray path, V_r, V_θ, and V_ϕ are the components of the wave normal direction, and μ and μ' are the phase and group refractive indices. Integration of the first three equations determines the location of the ray path in space while integration of the last three equations determines the components of the wave normal direction. Additional equations enable calculation of phase path, absorption, and other parameters which may be integrated along the ray path. The independent variable, t, is group path rather than phase path as used by Hazelgrove.

The remainder of the ray trace program, i.e., the initial aiming of the ray, the homing of the ray on the observer, the computation of the dispersive phase, etc., employs some of the techniques from earlier, Snell's Law ray tracing programs (R.S. Lawrence and D. J. Posakony, 1961; G. A. Dulk and W. A. Dean, 1962). When tracing the so-called "indirect rays", the initial aiming direction is toward a point slightly below the cloud center. For "direct rays" the initial direction is toward the observer. In each case, the ray is traced until it reaches the "impact

plane", a plane through the observer and perpendicular to the transmitter-observer line. The distance by which the impact point misses the observer (the miss distance) is used to compute a new aiming direction and another ray is traced. This process, called homing, is repeated until the miss distance is less than a predetermined amount.

Dispersive phase is computed by averaging the ordinary and extra-ordinary phase paths at the 36 and the 146 MHz frequencies. The phase path average at 36 MHz is multiplied by four and subtracted from the 146 MHz phase path average. The result is multiplied by two and this quantity is termed dispersive phase.

The changes in signal strength as a result of focusing and defocusing are measured in the following way. A ray at the frequency under consideration is traced through the unperturbed ionosphere until it homes on the observer. The starting direction of the ray is then deviated by 1/10 milliradian in each of three mutually perpendicular planes. The three rays so defined are traced to the impact plane and the area of the triangle whose vertices are the impact points is computed. The entire process is then repeated with the electron density perturbation due to the barium cloud included. The ratio of the triangle areas with and without the cloud is computed and expressed in decibels as a measure of signal reduction or enhancement due to the cloud.

Unclassified
Security Classification

DOCUMENT CONTROL DATA - R & D

(Security classification of title, body of abstract and indexing annotation must be entered when the overall report is classified)

1 ORIGINATING ACTIVITY (Corporate author)	2a. REPORT SECURITY CLASSIFICATION
U. S. Army Aberdeen Research and Development Center Ballistic Research Laboratories Aberdeen Proving Ground, Maryland 21005	Unclassified 2b. GROUP

3 REPORT TITLE

ELECTRON CONTENT OF BARIUM PLASMAS IN THE HIGH ATMOSPHERE

4 DESCRIPTIVE NOTES (Type of report and inclusive dates)

5 AUTHOR(S) (First name, middle initial, last name)

Raymond E. Prenatt
William V. Dean
Warren W. Berning

6 REPORT DATE	7a. TOTAL NO OF PAGES	7b. NO OF REFS
December 1969	55	18

8a. CONTRACT OR GRANT NO	9a. ORIGINATOR'S REPORT NUMBER(S)
b. PROJECT NO RDTL 5910.21.61083	BRL Report No. 1459
c.	9b. OTHER REPORT NO(S) (Any other numbers that may be assigned this report)
d.	

10 DISTRIBUTION STATEMENT

This document has been approved for public release and sale; its distribution is unlimited.

11 SUPPLEMENTARY NOTES	12 SPONSORING MILITARY ACTIVITY
This research was partially supported by Air Force Cambridge Research Laboratories	U. S. Army Materiel Command Washington, D. C. 20315

13. ABSTRACT

At evening twilight on 4 October 1967 a rocket carrier released three barium clouds off Wallops Island, Virginia. The vehicle also carried a multifrequency VHF beacon for the observation of radio frequency dispersive phase and amplitude variations in signals propagated through the release clouds, and as a derived quantity, total electron content along the propagation paths. The first cloud, at 103 kilometers, introduced no measurable dispersive phase variations and only a brief decrease in signal strength. The other clouds at 187 and 226 kilometers produced large and unusual effects on both dispersive phase and signal strength data.

Analysis of the dispersive phase data obtained during rocket descent, when the rocket had emerged from behind the release clouds, yielded a normal electron density profile. A preliminary attempt at interpreting the data relevant to the second release employed ray tracing through spherically symmetric, diffusing cloud models with a gaussian electron density distribution. By varying the parameters defining the cloud, a model was devised that closely duplicated both the dispersive phase and signal strength data.

DD FORM 1 NOV 68 1473 REPLACES DD FORM 1473, 1 JAN 64, WHICH IS OBSOLETE FOR ARMY USE.

Unclassified
Security Classification

Unclassified

Security Classification

4 KEY WORDS	LINK A		LINK B		LINK C	
	ROLE	WT	ROLE	WT	ROLE	WT
Barium Ion Clouds						
Chemical Releases in the Upper Atmosphere						
Dispersive Doppler						
Electron Content in Ion Clouds						
Ion Cloud Models						
Ionosphere						
Multifrequency Propagation Experiment						